THE JOURNAL OF PHYSICAL CHEMISTRY B

ARTICLE

pubs.acs.org/JPCB

Probing Side-Chain Dynamics in Proteins by the Measurement of Nine Deuterium Relaxation Rates Per Methyl Group

Xinli Liao,[†,§] Dong Long,[‡] Da-Wei Li,[‡] Rafael Brüschweiler,[‡] and Vitali Tugarinov*[,†]

[†]Department of Chemistry and Biochemistry, University of Maryland, College Park, Maryland 20742, United States

[‡]Chemical Sciences Laboratory, Department of Chemistry and Biochemistry and the National High Magnetic Field Laboratory, Florida State University, Tallahassee, Florida 32306, United States

Supporting Information

ABSTRACT: We demonstrate the feasibility of the measurement of up to nine deuterium spin relaxation rates in $^{13}CHD_2$ and $^{13}CH_2D$ methyl isotopomers of small proteins. In addition to five measurable ^2H relaxation rates in a $^{13}CH_2D$ methyl group (Millet, O.; Muhandiram, D. R.; Skrynnikov, N. R.; Kay, L. E. J. Am. Chem. Soc. 2002, 124, 6439−48), the measurement of additional four rates of (nearly) single-exponentially decaying magnetization terms in methyl groups of the $^{13}CHD_2$ variety is reported. Consistency relationships between ^2H spin relaxation rates measured in the two different types of methyl groups are derived and verified experimentally for a subset of methyl-containing side chains in the protein ubiquitin. A detailed comparison of methyl-bearing side-chain dynamics parameters obtained from relaxation measurements in $^{13}CH_2D$ and $^{13}CHD_2$ methyls of ubiquitin at 10, 27, and 40 °C reveals that transverse ^2H relaxation rates in $^{13}CHD_2$ groups are reliable and accurate reporters of the amplitudes of methyl 3-fold axis motions (S_{axis}^2) for protein molecules with global molecular tumbling times $\tau_C > \sim 9$ ns. For smaller molecules, simple correction of transverse ^2H relaxation rates in $^{13}CHD_2$ groups is sufficient for the derivation of robust measures of order. Residue-specific distributions of S_{axis}^2 are consistent with atomic-detail molecular dynamics (MD) results. Both $^{13}CHD_2$- and $^{13}CH_2D$-derived S_{axis}^2 values are in good overall agreement with those obtained from 1 μs MD simulations at all the three temperatures, although some differences in the site-specific temperature dependence between MD- and ^2H-relaxation-derived S_{axis}^2 values are observed.

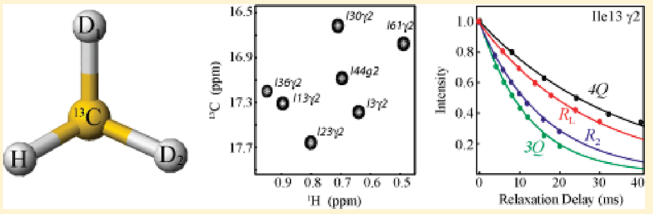

INTRODUCTION

The dynamics of protein molecules is often critical for their function.[1−5] Interactions between the structural motifs of single proteins as well as between different components of complex molecular assemblies are most often mediated through side chains of the participating amino acids. Dynamics of protein side chains is one of the major components of molecular recognition events,[6−9] as well as conformational entropy in the structures of folded proteins.[10−13] Solution NMR spectroscopy in general, and ^2H NMR spin relaxation techniques in particular, are especially powerful tools for the studies of side-chain mobility in proteins as detailed and easily interpretable information can be obtained on a site-specific basis under experimental conditions relevant for the function. Because deuterium NMR spin relaxation is dominated by a strong quadrupolar interaction,[14] and is largely impervious to contributions from other nuclear relaxation mechanisms including chemical exchange,[15−18] ^2H nuclei are recognized as the most reliable spin probes of side-chain dynamics in proteins.[19] Practically, the knowledge of only a single parameter, the anisotropy of the ^2H quadrupolar tensor or quadrupolar coupling constant, is required for the interpretation of ^2H relaxation data in terms of amplitudes and time scales of side-chain motions. This has stimulated the development of solution NMR techniques for the measurement of ^2H relaxation rates in the side chains of proteins in the past 15 years,[15,16,20] the main targets of NMR investigations being methyl groups of the $^{13}CH_2D$ variety,[15,16,18,20−27] methylene ^{13}CHD sites,[28] and ^{15}NHD moieties of Asn and Gln side chains.[29]

The choice of $^{13}CH_2D$ spin systems in the previous ^2H spin relaxation studies in methyl groups of small proteins is well justified,[15] as the presence of only a single deuteron makes the construction of experiments that quantify single-exponential decays of the terms of interest—e.g., spin relaxation of the transverse (longitudinal) ^2H terms $D_+(D_Z)$—relatively straightforward. In contrast, in the case of $^{13}CHD_2$ moieties a more complex mixture of terms that depends on products of operators of the two magnetically equivalent deuterons is obtained that significantly complicates analysis of NMR relaxation data in terms of motional characteristics. All the more so since ^2H spin relaxation in fast-rotating $^{13}CHD_2$ groups is generally not single exponential.[30,31] While ^2H relaxation in $^{13}CHD_2$ methyls was used on many occasions previously as a probe of side-chain mobility via the

Received: September 26, 2011
Revised: November 17, 2011
Published: November 18, 2011

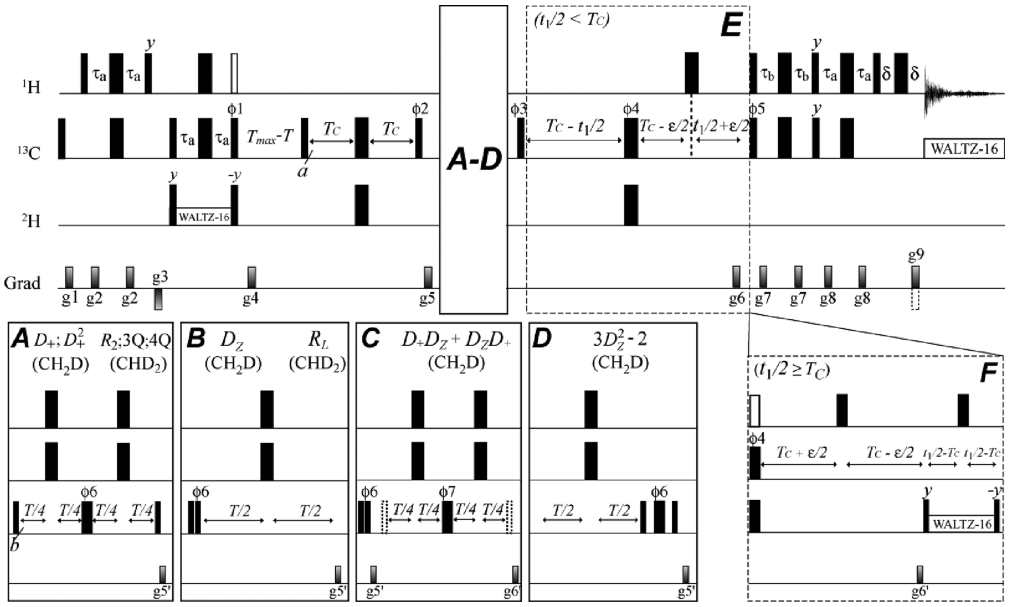

Figure 1. Pulse scheme for the measurement of ^{2}H relaxation rates in selectively ^{13}C-labeled $^{13}CH_2D$ and $^{13}CHD_2$ methyl groups of proteins from a series of gradient sensitivity enhanced 2D $^1H-^{13}C$ correlation maps produced via parametric variation of relaxation delay T (from 0 to T_{max}). The experimental details are described in Materials and Methods.

measurements of transverse (R_2) and longitudinal (R_L) rates in high-molecular-weight proteins (with global molecular tumbling time τ_C above 40 ns),[7,9,18,32−34] and the utility of $^{13}CHD_2$ methyls has been demonstrated in a variety of NMR applications to larger proteins,[35−38] no rigorous justification has been provided to date for the general validity of ^{2}H probes of dynamics in $^{13}CHD_2$ groups of smaller proteins where the contributions of high-frequency components to the generally non-single-exponential decays are expected to be significant. This is especially true with respect to R_2 measurements in $^{13}CHD_2$ methyls,[18] as these relaxation rates are single exponential only in methyl groups attached to large protein molecules and are the main reporters of the amplitudes of methyl 3-fold axis motions usually expressed as generalized order parameters S^2_{axis}.

We demonstrate here the feasibility of the measurement of up to nine ^{2}H spin relaxation rates in $^{13}CH_2D$ and $^{13}CHD_2$ methyl isotopomers together. In addition to five measurable ^{2}H relaxation rates in single-deuteron $^{13}CH_2D$ methyl groups,[16] the measurement of the additional four rates of (nearly) single-exponentially decaying magnetization terms in methyls of the $^{13}CHD_2$ variety is described. Using rigorous analysis of ^{2}H spin relaxation in fast-rotating $(^{13}CH)D_2$ spin systems, we derive "consistency" relationships between ^{2}H relaxation rates measured in the two types of methyl isotopomers and verify them experimentally on a sample of the 8.5 kDa protein ubiquitin selectively ^{13}C-labeled at $Ile^{\gamma 2}$, Val^{γ}, Leu^{δ}, Ala^{β}, and Met^{ε} methyl positions. A comparison of methyl-bearing side-chain dynamics parameters obtained from relaxation measurements in $^{13}CH_2D$ and $^{13}CHD_2$ methyls of ubiquitin at 10, 27, and 40 °C reveals that ^{2}H relaxation rates in $^{13}CHD_2$ methyls provide reliable estimates of S^2_{axis} for protein molecules with tumbling times higher than ∼9 ns. For smaller molecules, a simple correction of the ^{2}H R_2 relaxation rates in $^{13}CHD_2$ groups or the $^{13}CHD_2$-derived S^2_{axis} values may be used to obtain quantitatively reliable estimates of side-chain order. Residue-specific distributions of both $^{13}CHD_2$- and $^{13}CH_2D$-derived S^2_{axis} are consistent with side-chain rotameric preferences derived from molecular dynamics (MD) simulations.[39] Although some differences in the temperature dependence between ^{2}H-relaxation-derived S^2_{axis} values and those obtained from 1 μs MD simulations of ubiquitin are noted, ^{2}H-relaxation derived S^2_{axis} values and especially the patterns of S^2_{axis} variation along the protein sequence are in very good agreement with those obtained from MD simulations at all the three temperatures.

MATERIALS AND METHODS

NMR Sample. The sample of wild-type human ubiquitin used in this work has been obtained using [3-$^{13}C_1$]-pyruvate (Isotec/Sigma-Aldrich, Miamisburg, OH) as the principal carbon source in 99% D_2O-based minimal medium.[40−42] This labeling strategy leads to approximately equal populations of selectively ^{13}C-labeled methyl isotopomers of $^{13}CHD_2$ and $^{13}CH_2D$ variety at $Ile^{\gamma 2}$, Val^{γ}, Leu^{δ}, Ala^{β}, and Met^{ε} positions, allowing for ^{2}H relaxation measurements in isotopomers of both types in the same protein sample. Approximately the same isotope labeling pattern can be achieved using [1-$^{13}C_1$]-glucose as the main carbon source in D_2O-based medium albeit with >50% losses in ^{13}C enrichment of methyl groups.[43,44] The [3-$^{13}C_1$]-pyruvate-derived sample of ubiquitin was 2.0 mM in protein concentration and was dissolved in 99.9% D_2O sodium phosphate buffer (pD = 6.8, uncorrected) containing 0.03% NaN_3 and a set of protease inhibitors.

Deuterium Relaxation Measurements. All NMR experiments were performed on a 600 MHz Bruker Avance III spectrometer equipped with a room temperature triple-resonance z-gradient probe. The measurements of ^{2}H relaxation rates in $^{13}CHD_2$ and $^{13}CH_2D$ methyl groups (nine rates in total) of the [3-$^{13}C_1$]-pyruvate-derived sample of ubiquitin have been performed at 10, 27, and 40 °C via the gradient sensitivity-enhanced pulse scheme of Figure 1 using the following set of experimental parameters. All narrow(wide) rectangular pulses are applied with flip angles of 90(180)° along the x-axis unless

dx.doi.org/10.1021/jp209304c | J. Phys. Chem. B 2012, 116, 606–620

indicated otherwise. The ^{1}H, ^{2}H, and ^{13}C carrier frequencies are positioned in the center of the methyl region at 1, 1, and 22 ppm, respectively. All ^{1}H and ^{13}C pulses are applied with the highest possible power, while a 2.9 kHz field is used for ^{2}H pulses. ^{2}H(^{13}C) WALTZ-16[45] decoupling uses a 0.9(2.4) kHz field. Delays are as follows: $\tau_a = \varepsilon = 1/(4J_{CH}) = 2.0$ ms; $\delta = 400$ μs; $\tau_b = 1/(4J_{CH}) = 2.0$ ms for $^{13}CHD_2$ measurements, and $\tau_b = 1/(6J_{CH}) = 1.3$ ms for $^{13}CH_2D$ methyls.[46] Delay $T_C = 1/(8J_{CD}) = 6.0$ ms for "rank-1" measurements in $^{13}CH_2D$ methyls; $T_C = 1/(4J_{CD}) = 12.0$ ms for all "rank-2" measurements in $^{13}CH_2D$ and R_{4Q} rates in $^{13}CHD_2$ methyls; $T_C = 9.0$ ms ($\sim 1/6J_{CD}$)[32] for R_L and R_{3Q} measurements, and $T_C = 1/(12J_{CD}) = 4$ ms for R_2 measurements in $^{13}CHD_2$ groups. Insets A−D show the elements of the scheme used for different ^{2}H rate measurements in methyl isotopomers indicated in parentheses. The pulses shown with dashed rectangles in inset C have 45° flip angles. Inset F is used for all the measurements when $t_1/2 \geq T_C$. Open 90° ^{1}H pulse is applied only for the rate measurements in $^{13}CHD_2$ groups, while the open 180° ^{1}H pulse in inset F is applied only for the rate measurements in $^{13}CH_2D$ methyls. The phase cycle is as follows: $\phi1 = y$ for $^{13}CHD_2$ and $\phi1 = x$ for $^{13}CH_2D$ groups; $\phi2 = y$ for all rank-1 measurements in $^{13}CH_2D$ methyls and R_{3Q}, R_L measurements in $^{13}CHD_2$ groups, while $\phi2 = x$ for all rank-2 measurements in $^{13}CH_2D$ and R_{4Q} measurements in $^{13}CHD_2$ groups; $\phi3 = x,-x$ for R_{3Q}, R_L in $^{13}CHD_2$ and rank-2 measurements in $^{13}CH_2D$ groups, while $\phi3 = y,-y$ for R_{4Q} in $^{13}CHD_2$ and rank-1 measurements in $^{13}CH_2D$ groups; $\phi4 = 4(x), 4(-x)$; $\phi5 = x$; $\phi6 = [2(x), 2(y), 2(-x), 2(-y); 2(0°), 2(45°), 2(90°), 2(135°); 2(0°), 2(30°), 2(60°), 2(90°), 2(120°), 2(150°)$, and $2(22.5°), 2(45°), 2(67.5°), 2(90°), 2(112.5°), 2(135°), 2(157.5°), 2(180°)]$ for $[R(D_+); R(D_+^2); R_{3Q}$, and $R_{4Q}]$ measurements, respectively (inset A); $\phi6 = 2(x),2(-x)$ (inset B); $\phi6 = x,-x$; $\phi7 = 2(x), 2(y), 2(-x), 2(-y)$ (inset C); $\phi6 = 2(0°), 2(45°), 2(90°), 2(135°)$ (inset D); rec. $= x,-x,-x,x$. Quadrature detection in F_1 is achieved with a gradient enhanced sensitivity scheme[47,48] by recording a pair of data sets with ($\phi5$; g9) and ($-\phi5$; $-$g9) for each t_1 point. For each successive t_1 value, $\phi3$ is inverted.[49] Durations and strengths of pulsed-field gradients in units of (ms; G/cm) are as follows: g1 = (1; 15); g2 = (0.3; 5); g3 = (1.2; −12); g4 = (0.5; 15); g5 = (0.7; 12); g6 = (0.5; 25); g7 = (0.4; 15); g8 = (0.3; 10); g9 = (0.1252; 25); g5′ = (0.6; 10); g6′ = (0.8; 12).

All NMR data sets were composed of [150,512] complex points in the [^{13}C,^{1}H] dimensions with corresponding acquisition times of [80 ms,64 ms]. The recovery delay of 1.4(1.7) s was used in the measurements performed on $^{13}CH_2D$($^{13}CHD_2$) isotopomers. The recording of 16 scans/FID in all measurements except $R_{3Q}(CHD_2)$ and $R_{4Q}(CHD_2)$ resulted in net acquisition times of ∼117(140) min/experiment for $^{13}CH_2D$($^{13}CHD_2$) methyls. For $R_{3Q}(CHD_2)$ and $R_{4Q}(CHD_2)$ rate measurements, 64 scans/FID were collected resulting in net acquisition times of ∼9.5 h/experiment. Six or seven time points (relaxation delays T) were acquired in each of the measurements with one additional point repeated for error estimation.

Data Analysis. All NMR spectra were processed using the NMRPipe/NMRDraw suite of programs and associated software.[50] ^{2}H relaxation rates were obtained by fitting peak intensities to a single-exponential function of the form $I = I_0 \exp(-RT)$, where I is the measured intensity and R is the relaxation rate. Errors in peak intensities have been estimated from duplicate measurements and subsequently propagated to the errors in the extracted rates using Monte Carlo analysis.[51]

Earlier, Millet et al. developed experiments for the measurement of five deuterium relaxation rates in $^{13}CH_2D$ methyl groups of [U-^{13}C]-labeled proteins.[16] These rates quantify the relaxation of D_+, D_Z (rank-1) and $D_+D_Z + D_ZD_+$, $3D_Z^2 - 2$, D_+^2 (rank-2) ^{2}H magnetization modes. The quadrupolar relaxation rates of these five elements are given by[15,16,52]

$$R(D_+; CH_2D) = \left(\frac{1}{80}\right)(2\pi QCC)^2[9J(0) + 15J(\omega_D) + 6J(2\omega_D)] \quad (1a)$$

$$R(D_Z; CH_2D) = \left(\frac{3}{40}\right)(2\pi QCC)^2[J(\omega_D) + 4J(2\omega_D)] \quad (1b)$$

$$R(D_+D_Z + D_ZD_+; CH_2D) = \left(\frac{1}{80}\right)(2\pi QCC)^2[9J(0) + 3J(\omega_D) + 6J(2\omega_D)] \quad (1c)$$

$$R(3D_Z^2 - 2; CH_2D) = \left(\frac{3}{40}\right)(2\pi QCC)^2[3J(\omega_D)] \quad (1d)$$

$$R(D_+^2; CH_2D) = \left(\frac{3}{40}\right)(2\pi QCC)^2[J(\omega_D) + 2J(2\omega_D)] \quad (1e)$$

where spin operator $D_+ = D_x + iD_y$, QCC = (e^2qQ/h) is a quadrupolar coupling constant equal to 167 kHz in methyl deuterons.[53] $J(\omega)$ is the spectral density function which in its simplest model-free form,[20,54,55] is given by

$$J(\omega) = \frac{1}{9}S_{axis}^2\left(\frac{A_1\tau_1}{1 + (\omega\tau_1)^2} + \frac{A_2\tau_2}{1 + (\omega\tau_2)^2} + \frac{A_3\tau_3}{1 + (\omega\tau_3)^2}\right) + \left(P_2(\cos\alpha) - \frac{1}{9}S_{axis}^2\right)\frac{\tau_e}{1 + (\omega\tau_e)^2} \quad (2a)$$

where S_{axis}^2 is the generalized order parameter of the methyl 3-fold symmetry axis; $P_2 = (1/2)[3\cos^2(x) - 1]$; angle α is formed by the principal axes of the electric field gradient (EFG) tensors of the two deuterons in $^{13}CHD_2$ groups: i.e., $\alpha = 0°$ and $P_2(\cos\alpha) = 1$ for all $^{13}CH_2D$ methyl rates (eqs 1a−1e) and for the autocorrelation spectral density function in $^{13}CHD_2$ methyls, $J^A(\omega)$, while under the assumption of ideal tetrahedral methyl geometry $\alpha = 109.5°$ and $P_2(\cos\alpha) = -1/3$ for the quadrupolar cross-correlation spectral density function in $^{13}CHD_2$ groups, $J^C(\omega)$; $A_1 = (3/4)\sin^4(\theta)$, $A_2 = 3\sin^2(\theta)\cos^2(\theta)$, $A_3 = [(3/2)\cos^2(\theta) - 0.5]^2$, $\tau_1 = (4D_\parallel + 2D_\perp)^{-1}$, $\tau_2 = (D_\parallel + 5D_\perp)^{-1}$, $\tau_3 = (6D_\perp)^{-1}$, $D_\parallel$ and $D_\perp$ are the principal components of the molecular diffusion tensor, θ is the angle between the $^{13}C_m$−C bond vector and the unique molecular diffusion axis, and $1/\tau_e = 1/\tau_f + 1/\tau_{c,eff}$, where $\tau_{c,eff} = (2D_\parallel + 4D_\perp)^{-1}$ is the effective correlation time of overall rotation, and τ_f is the correlation time of (fast) local motions. Direction cosines for methyl $^{13}C_m$−C bond vectors have been obtained from the crystal structure of ubiquitin (PDB code 1ubq[56]).

The values of $\tau_e(\tau_f)$ in eq 2a represent in a complex way an "amalgam" of the time scales of all motional processes that affect methyl R_1 relaxation including fast methyl rotation.[15,20,57] Separation of the time scales of fast methyl rotation and generally

slower motions of the methyl 3-fold axis (C−C bond vector) can be achieved using the parametrization of the spectral density suggested by Showalter et al.[58] The following expression for the spectral density function was used for detection of slow (high picosecond to low nanosecond) time-scale motions:[58,59]

$$J(\omega) = S_f^2\left\{S_{CC}^2\left(\frac{1}{9}\left[\frac{\tau_c}{1+\omega^2\tau_c^2}\right] + \frac{8}{9}\left[\frac{\tau_{CH_3,c}}{1+\omega^2\tau_{CH_3,c}^2}\right]\right) + (P_2(\cos\alpha) - S_{CC}^2)\left(\frac{1}{9}\left[\frac{\tau_{CC,c}}{1+\omega^2\tau_{CC,c}^2}\right] + \frac{8}{9}\left[\frac{\tau_{CH_3,CC,c}}{1+\omega^2\tau_{CH_3,CC,c}^2}\right]\right)\right\} \quad (2b)$$

where S_f^2 is an order parameter belonging to very rapid librational motions (<1 ps), typically ~0.86 (see text), S_{CC}^2 is an order parameter that describes rotameric jumps (reorientation of the C−C bond vector), $\tau_{CH_3,c}^{-1} = \tau_{CH_3}^{-1} + \tau_c^{-1}$, $\tau_{CC,c}^{-1} = \tau_{CC}^{-1} + \tau_c^{-1}$, $\tau_{CH3,CC,c}^{-1} = \tau_{CH3}^{-1} + \tau_{CC}^{-1} + \tau_c^{-1}$, $\tau_c = \sum_{i=1}^{3} A_i\tau_i$ is the overall tumbling correlation time with A_i and τ_i defined as in eq 2a, τ_{CC} is the correlation time of the rotameric jumps, and τ_{CH3} is the correlation time of methyl rotation about the 3-fold symmetry axis.[58] The form of $J(\omega)$ in eq 2b is very similar to the extended model-free expression[60] for methyl groups used in a number of previous studies.[20,27,42,61,62]

Accurate parameters of the global rotational diffusion tensor of ubiquitin at 10, 27, and 40 °C were obtained previously from the backbone amide ^{15}N and $^2H^\alpha$ relaxation data.[63] Since the sample used in this study for ^{2}H relaxation measurements was dissolved in D_2O, for derivation of methyl dynamics parameters effective molecular reorientation times $\tau_{c,eff}$ have been scaled by the ratios of D_2O/H_2O viscosities at each of the three temperatures:[64] $\tau_{c,eff}(D_2O;°T) = [\eta^{D2O}/\eta^{H2O}](°T)\tau_{c,eff}(H_2O;°T)$, leading to $\tau_{c,eff}$ = (8.9; 5.0; 3.6) ns for ubiquitin in D_2O at (10; 27; 40)°C. Anisotropy of the diffusion tensor of ubiquitin $D_\parallel/D_\perp = 1.18$ was used at all temperatures along with the polar angles defining the orientation of the molecular diffusion tensor with respect to the inertial coordinate frame $\theta = 6°$ and $\phi = -16°$.[63,65]

Molecular Dynamics Simulations. Two 1 μs MD trajectories of ubiquitin at 10 and 40 °C were generated in the present work for side-chain dynamics analysis, in addition to the previously published 1 μs trajectory at 27 °C,[66] using the GROMACS[67] software package version 4.5.3 with TIP3P explicit water model[68] and the ff99SBnmr1-ILDN force field.[66] The GROMACS force-field files for ff99SBnmr1-ILDN were modified from those of ff99SB-ILDN[69] (included in the current version of the software package) by incorporating the ff99SBnmr1 backbone parameters.[70] The setup of the simulations was fully analogous to the protocol described previously.[66,71] The generalized order parameters S^2 for the axial C−C bond vectors were back-calculated from the three 1 μs time scale trajectories using the method described previously[66] over a range of averaging windows of 1, 3, 5, 7, 10, and 15 ns length, followed by comparison with experimentally derived S_{axis}^2 values.

RESULTS AND DISCUSSION

Experimental Setup for ^{2}H Relaxation Measurements in $^{13}CH_2D$ and $^{13}CHD_2$ Methyls. The measurements of five deuterium spin relaxation rates in $^{13}CH_2D$ methyl groups of [U-^{13}C]-labeled small proteins have been described by Millet et al.[16] The relaxation rates of rank-1 (D_+, D_Z) and rank-2 (D_+D_Z + D_ZD_+, $3D_Z^2 - 2$, and D_+^2) deuterium spin operators can be measured in protein samples *selectively* ^{13}C-labeled at methyl positions using the pulse scheme of Figure 1. This experiment is based on the gradient sensitivity enhanced scheme developed for ^{2}H relaxation measurements in $^{13}CHD_2$ groups of selectively ^{13}C-methyl-labeled large proteins.[18,19,32] The distinct advantage of the scheme in Figure 1 is the possibility of selection for and ^{2}H relaxation measurements in methyl isotopomers of both types ($^{13}CH_2D$ and $^{13}CHD_2$), with minimal modifications of the pulse sequence needed to "switch" the measurements between these two types of methyl groups (see Materials and Methods for details).

As in ^{2}H relaxation experiments developed earlier, the magnetization flow follows the path $^1H \rightarrow {}^{13}C \rightarrow {}^2H(T) \rightarrow {}^{13}C(t_1) \rightarrow {}^1H(t_2)$, where the transfer from one spin to the next is achieved via one-bond scalar couplings and t_1, t_2 are acquisition periods. A series of 2D methyl ^{1}H−^{13}C correlation maps are recorded as a function of parametrically varied delay T, and the ^{2}H relaxation rates, R, are extracted from the fit of cross-peak intensities to a two-parameter single-exponential function. As it is the case in other ^{2}H relaxation measurements,[16,18] this provides the decay rates of $2H_ZC_Z[D]$ and $C_Z[D]$ magnetization terms in $^{13}CH_2D$ and $^{13}CHD_2$ isotopomers, respectively, where $[D]$ is a deuterium-containing magnetization term. The pulse scheme of Figure 1 allows for subtraction of the contributions of the $2H_ZC_Z(C_Z)$ rates in $^{13}CH_2D(^{13}CHD_2)$ groups from $2H_ZC_Z[D](C_Z[D])$ rates "on-the-fly" by including the element of duration $T_{max} - T$.[16,18] Selective ^{13}C labeling at methyl positions—though not absolutely necessary in applications to small proteins—provides certain flexibility in the design of the experiment at the expense of the loss of correlations belonging to Thr$^{\gamma 2}$ and Ile$^{\delta 1}$ methyl groups. Specifically, the maximal acquisition time and the resulting resolution in t_1 are not limited to multiples of $1/J_{CC}$ where J_{CC} is the ^{13}C−^{13}C coupling in [U-^{13}C]-labeled samples (see inset F used in Figure 1 for $t_1/2 \geq T_C$). In addition, strong $^{13}C\delta-{}^{13}C\gamma$ couplings possible in [U-^{13}C]-labeled leucine side chains do not complicate relaxation measurements in selectively ^{13}C-methyl-labeled samples.

Since the experimental basis of five rank-1 and rank-2 relaxation rate measurements in $^{13}CH_2D$ groups was described in detail previously,[15,16] here we concentrate exclusively upon the measurements of four relaxation relates in $^{13}CHD_2$ isotopomers. It can be shown that the evolution of the in-phase magnetization C_y present at time point a of the pulse scheme (Figure 1), during the $2T_C$ period due to one-bond C−D scalar coupling, J_{CD}, can be written as $C_y \rightarrow (L_1 + L_1') + (L_2 + L_2') + L_3$, where L_i are the five components of the $^{13}C(H)D_2$ pentet L_1:L_2:L_3:L_2':L_1' given by (see also Muhandiram et al.[15])

$$L_1 + L_1' = 0.5C_y(D_{Z,1}^2D_{Z,2}^2 + D_{Z,1}D_{Z,2})\cos(8\pi J_{CD}T_C) - 0.5C_x(D_{Z,1}^2D_{Z,2} + D_{Z,1}D_{Z,2}^2)\sin(8\pi J_{CD}T_C) \quad (3a)$$

$$L_2 + L_1' = C_y(D_{Z,1}^2 + D_{Z,2}^2 - 2D_{Z,1}^2D_{Z,2}^2)\cos(4\pi J_{CD}T_C) - C_x(D_{Z,1} + D_{Z,2} - D_{Z,1}^2D_{Z,2} - D_{Z,1}D_{Z,2}^2)\sin(4\pi J_{CD}T_C) \quad (3b)$$

$$L_3 = C_y(1 - D_{Z,1}^2 - D_{Z,2}^2 + 1.5D_{Z,1}^2D_{Z,2}^2 - 0.5D_{Z,1}D_{Z,2}) \quad (3c)$$

where C and D are product operators of ^{13}C and ^{2}H nuclei, respectively, and the subscripts 1 and 2 distinguish the two deuteron spins. The application of ^{13}C 90°$_{\phi 2}$ pulse with the phase

$\phi 2 = y$ followed by the gradient g5 and the ^{2}H 90°$_x$ pulse, leads to selection of the terms in eqs 3a−3c containing C_x operators only, resulting in the following terms of interest at point b of the scheme (Figure 1; inset A):

$$-C_z(D_{y,1} + D_{y,2})\sin(4\pi J_{CD}T_C) - C_z(D_{y,1}^2 D_{y,2} + D_{y,1}D_{y,2}^2)[0.5\sin(8\pi J_{CD}T_C) - \sin(4\pi J_{CD}T_C)] \quad (4)$$

In the single-transition basis derived from the energy level diagram of the (^{13}CH)D$_2$ spin system shown in Figure 2, the magnetization in (4) corresponds to the superposition of single-quantum (SQ) and triple-quantum (3Q) ^{2}H coherences:

$$iC_z([\rho_{1-2} + \rho_{4-5} + 0.5\sqrt{6}(\rho_{2-3} + \rho_{3-4}) + 0.5\sqrt{2}(\rho_{5-6} + \rho_{6-7})]\sin(4\pi J_{CD}T_C) + [0.5(\rho_{1-2} + \rho_{4-5}) + 0.5\sqrt{6}(\rho_{2-3} + \rho_{3-4}) - 0.5(\rho_{1-4}^{3Q} + \rho_{2-5}^{3Q})](0.5\sin 8\pi J_{CD}T_C - \sin 4\pi J_{CD}T_C)) \quad (5)$$

The relaxation rate of the sum of all elements in expression 5 is denoted by $R_2(CHD_2)$. As it has been shown previously[18] and discussed in more detail below (see Deuterium Relaxation Rates in ^{13}CHD$_2$ Methyl Groups), $R_2(CHD_2)$ rates are single-exponential only in the "$J(0)$ limit", i.e., if $J(0) \gg J(\omega_D)$, $J(2\omega_D)$. Following the relaxation delay T, carbon chemical shifts are recorded, and carbon magnetization is refocused with respect to the coupled deuterons prior to the transfer to methyl protons for detection. The net transfer function for the "out-and-back" transfer process of all the elements in expression 5 is given by $2\sin^2(8\pi J_{CD}T_C) + 4\sin^2(4\pi J_{CD}T_C)$, and has a maximum when $T_C = 1/(12J_{CD})$.[25]

The sum of 3Q transitions in expression 5 can be selected in a straightforward manner by incrementing $\phi 6$ of the ^{2}H 180° pulse in the middle of the delay T in steps of 30° with the concomitant inversion of the receiver phase (Figure 1, inset A). The relaxation rate of the sum of 3Q terms ($\rho_{1-4}^{3Q} + \rho_{2-5}^{3Q} \equiv 0.25D_{\pm,1}^2 D_{\pm,2} + 0.25D_{\pm,1}D_{\pm,2}^2$) is denoted by $R_{3Q}(CHD_2)$ in what follows. The main rationale for this selection is that relaxation of 3Q transitions is single-exponential at all frequencies as described below. In favorable cases, it can be therefore used as a verification of the $R_2(CHD_2)$-derived measures of order. The net out-and-back transfer function for the 3Q terms only has a maximum at $T_C = 1/(6J_{CD})$ (see subsection Relative Sensitivities of Deuterium Relaxation Rate Measurements below).

It has been shown previously that for longitudinal relaxation measurements in ^{13}CHD$_2$ groups a magnetization mode can be constructed that relaxes single-exponentially to an excellent approximation: $M_L = C_z\{D_{z,1} + D_{z,2} - (3/2)(D_{z,1}D_{z,2}^2 + D_{z,2}D_{z,1}^2)\}$.[32] The decay rate of this magnetization mode M_L is referred to as $R_L(CHD_2)$ in this work. It can be measured using the scheme of Figure 1 (inset B), with the delay T_C adjusted to $1/(6J_{CD})$.[32]

Another set of coherences in the (^{13}CH)D$_2$ spin system can be selected if the ^{13}C 90°$_{\phi 2}$ pulse in Figure 1 is applied with $\phi 2 = x$ and the delay T_C is adjusted to $1/(4J_{CD})$, leading to the selection of magnetization terms in eqs 3a−3c that contain carbon spin operators C_y. After the application of the gradient g5 and the subsequent ^{2}H 90°$_x$ pulse, the resulting magnetization at point b in Figure 1 (inset A) is given by $C_Z(1 - 2D_{y,1}^2 + 2D_{y,2}^2 + 4D_{y,1}^2 D_{y,2}^2)$. Using the notation of the energy level diagram in Figure 2, this magnetization can be represented as a mixture of zero(ZQ)-, double(DQ)-, and quadruple(4Q)-quantum ^{2}H coherences: $C_z(\rho_{6-8}^{DQ} - \rho_{2-4}^{DQ} + \rho_{1-5}^{4Q} + ZQ)$, where ZQ denotes zero-quantum terms. While the relaxation of DQ terms is highly non-single-exponential at all frequencies including $J(0)$, the single 4Q transition $\rho_{1-5}^{4Q} \equiv 0.25D_{\pm,1}^2 D_{\pm,2}^2$ can be selected for (although at the expense of large losses in sensitivity as described below) by incrementing the phase $\phi 6$ of the ^{2}H 180° pulse in the middle of delay T in steps of 22.5° with the concomitant inversion of the receiver phase (Figure 1, inset A). In what follows, the relaxation rate of the 4Q terms is denoted by $R_{4Q}(CHD_2)$.

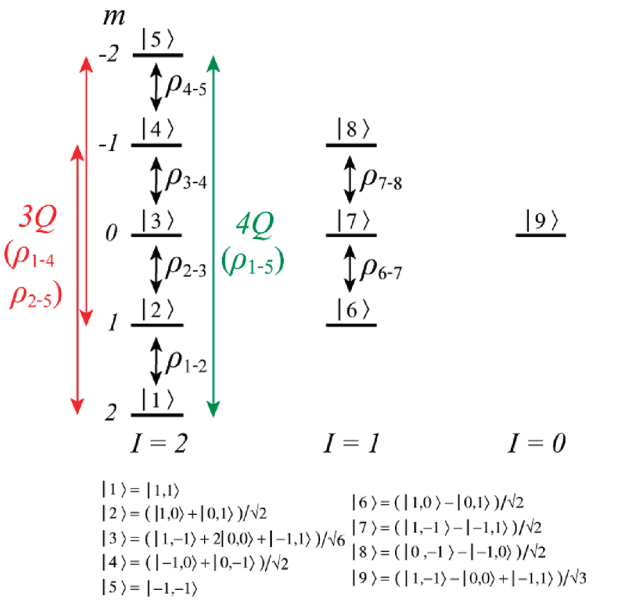

Figure 2. Energy level diagram for the (^{13}CH)D$_2$ spin system of a rapidly rotating ^{13}CHD$_2$ methyl group. Only two of the illustrated manifolds ($I = 2$ and $I = 1$) contribute to the signal in the experiments described in the text. ^{13}C and ^{1}H are treated as "silent" spins reducing the spin system to that of two coupled equivalent deuterons (D$_2$). Triple-quantum (3Q; $\Delta m = 3$) and quadruple quantum (4Q; $\Delta m = 4$) ^{2}H transitions are shown with red (green) arrows. Each eigenfunction $|i\rangle$, where $i = \{1,2,3,4,5,6,7,8,9\}$ is the wave function for the pair of magnetically equivalent deuterons. Single-quantum transitions between energy levels are denoted with ρ_{i-j}, where $\rho_{i-j} = (|i\rangle\langle j| + |j\rangle\langle i|)$, $i < j$. Expressions for the 3Q and 4Q relaxation rates in the spin system consisting of two equivalent deuterons (D$_2$) are given in the text.

Figure 3a shows a region of the methyl ^{1}H−^{13}C correlation map corresponding to the first point of the $R_{3Q}(CHD_2)$ measurement ($T = 0$), while typical decay curves of the four rates (R_2, R_L, R_{3Q}, and R_{4Q}) in ^{13}CHD$_2$ methyls of ubiquitin are shown in Figures 3b,c. The average measured (R_2; R_L; R_{3Q}; R_{4Q}) relaxation rates of (106.7; 43.8; 121.4; 31.6) s^{-1}; (64.8; 39.1; 79.3; 27.5) s^{-1}, and (48.9; 37.1; 64.2; 25.5) s^{-1} have been obtained in 32 ^{13}CHD$_2$ methyl groups of ubiquitin at 10, 27, and 40 °C, respectively. The average measured rates of (D_+; D_Z; $D_+D_Z + D_ZD_+$; $3D_Z^2 - 2$; D_+^2) in ^{13}CH$_2$D methyls for the same subset of residues are (104.5; 25.4; 91.7; 19.4; 15.4) s^{-1}; (62.6; 21.4; 51.6; 18.1; 13.6) s^{-1}, and (47.7; 19.6; 36.8; 17.6; 12.6) s^{-1} at 10, 27, and 40 °C, respectively. Below, we provide expressions for quadrupolar relaxation rates of $R_2(CHD_2)$, $R_L(CHD_2)$, $R_{3Q}(CHD_2)$, and $R_{4Q}(CHD_2)$ that have been used in all subsequent relaxation rate analyses.

Deuterium Relaxation Rates in ^{13}CHD$_2$ Methyl Groups. It has been shown previously that $R_2(CHD_2)$ is single-exponential

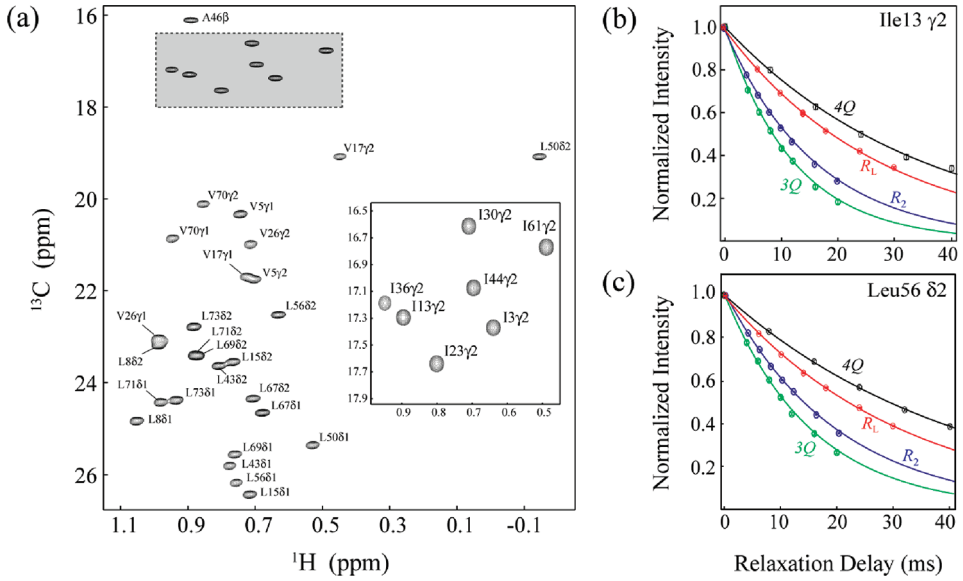

Figure 3. (a) A region of the methyl $^{1}H-^{13}C$ correlation map obtained with the pulse scheme of Figure 1 for the first point of R_{3Q} measurement in $^{13}CHD_2$ methyls (panel A) recorded on the [3-$^{13}C_1$]-pyruvate-derived ubiquitin (27 °C, 600 MHz). The shaded region of the map (Ile$^{\gamma 2}$ methyls) is enlarged in the inset. (b,c) Selected relaxation decay curves for the measurement of R_{3Q}, R_{4Q}, R_L, and R_2 rates in $^{13}CHD_2$ groups of (b) Ile13$^{\gamma 2}$ and (c) Leu56$^{\delta 2}$ methyls. Relaxation decay curves of $R_2(CHD_2)$ were best-fit to a monoexponential function.

only in the limit when $J(0) \gg J(\omega_D), J(2\omega_D)$ (i.e., it is not single-exponential at higher, ω_D and $2\omega_D$, frequencies).[18] $R_2(CHD_2)$ rates are commonly used as measures of methyl-containing side-chain dynamics in high-molecular-weight proteins where contributions from high-frequency components are negligible.[18,19,34] Using Redfield theory,[72] it is straightforward to calculate the relaxation matrices for all SQ transitions ρ_{i-j} in a (^{13}CH)D$_2$ group in Figure 2. These matrices are provided in the Supporting Information. Indeed, for the spectral density function evaluated at zero frequency, the relaxation matrix is diagonal with the relaxation rates equal to those of $R(D_+)$ magnetization in $^{13}CH_2D$ methyls, $(9/80)(2\pi QCC)^2J(0)$ (eq 1a). Usually, for extraction of motional parameters of methyl groups in large proteins, the $R_2(CHD_2)$ decay rates are fitted to the full expression for $R(D_+;CH_2D) = (1/80)(2\pi QCC)^2[9J(0) + 15J(\omega_D) + 6J(2\omega_D)]$ (eq 1a).[7,19,32,33] In this study, we provide rigorous justification for and define the range of applicability of eq 1a for extraction of motional parameters from R_2 rates in $^{13}CHD_2$ methyls.

Using full relaxation matrices, we have simulated $R_2(CHD_2)$ decay as a function of side-chain motional parameters $(S^2_{axis};\tau_f)$ and fitted the simulated curves to a single-exponential function (see Supporting Information for details). The comparison of the resulting rates with those calculated directly from the expression $(1/80)(2\pi QCC)^2[9J(0) + 15J(\omega_D) + 6J(2\omega_D)]$ is provided in Figure 4 in the form of contour plots showing relative errors of $R_2(CHD_2)$ (in %) as a function of $(S^2_{axis};\ \tau_f)$ for a set of isotropic global molecular reorientation correlation times, τ_C. The $R_2(CHD_2)$ rates are invariably larger than $R(D_+;CH_2D)$, although the increase is very small in the range of τ_C values between 4 and 10 ns: for the average set of motional parameters of methyls in ubiquitin obtained in this work ($S^2_{axis} = 0.6$; $\tau_f = 45$ ps) the relative errors vary between ~1.5% for $\tau_C = 10$ ns to ~3% for $\tau_C = 4$ ns. As expected, the "worst case" scenario is realized for the lowest correlation time where the contributions of the spectral density evaluated at high frequencies are the highest leading to 3−4% higher rates for low S^2_{axis} values (Figure 4a). Such a slight overestimation of the "true" rate due to high-frequency components of $R_2(CHD_2)$ is borne out by experimental data: the average ratio of $R_2(CHD_2)/R(D_+;CH_2D)$ rates for 32 methyls in ubiquitin at all three temperatures varies only in the range between 1.02 and 1.035. Since the differences between the measured $R_2(CHD_2)$ and $R(D_+;CH_2D)$ rates are very small for any $(S^2_{axis};\ \tau_f)$ sets of values, we have ascertained that the inequality $R_2(CHD_2) > R(D_+;CH_2D)$ holds in all methyls of ubiquitin even if the corresponding relaxation measurements are performed with the period $T_{max} - T$ set to a constant value (restricted to the duration of the gradient g5 and the following short gradient recovery delay, Figure 1). Because the relaxation rates of $2H_ZC_Z(2C_Z)$ magnetization are subtracted "on the fly" in the scheme of Figure 1, it is important to verify that the measured differences between $R_2(CHD_2)$ and $R(D_+;CH_2D)$ do not arise merely from this subtraction, especially so as the decay rate of $2H_ZC_Z$ terms (~2.0 s^{-1}) is ~2.5-fold higher on average than that of $2C_Z$ (~0.8 s^{-1}). Indeed, thus measured $R_2(CHD_2)$ rates remain on average 2% higher than their R_2 counterparts in $^{13}CH_2D$ methyl groups.

The evolution of higher order (3Q and 4Q) ^{2}H coherences in (^{13}CH)D$_2$ groups during delay T can be expressed as

$$\frac{d}{dT}\begin{bmatrix}\rho^{3Q}_{1-4}+\rho^{3Q}_{2-5}\\ \rho^{3Q}_{1-4}-\rho^{3Q}_{2-5}\end{bmatrix} = -\left(\frac{1}{80}\right)(2\pi QCC)^2\left[\begin{pmatrix}9&0\\0&9\end{pmatrix}J^A(0) + \begin{pmatrix}21&0\\0&9\end{pmatrix}J^A(\omega_D) + \begin{pmatrix}12&0\\0&0\end{pmatrix}J^C(\omega_D) + \begin{pmatrix}18&0\\0&18\end{pmatrix}J^A(2\omega_D)\right]\begin{bmatrix}\rho^{3Q}_{1-4}+\rho^{3Q}_{2-5}\\ \rho^{3Q}_{1-4}-\rho^{3Q}_{2-5}\end{bmatrix} \quad (6)$$

and

$$\frac{d}{dT}[\rho^{4Q}_{1-5}] = -\left(\frac{3}{40}\right)(2\pi QCC)^2[2J^A(\omega_D) + 4J^A(2\omega_D)][\rho^{4Q}_{1-5}] \quad (7)$$

dx.doi.org/10.1021/jp209304c |J. Phys. Chem. B 2012, 116, 606–620

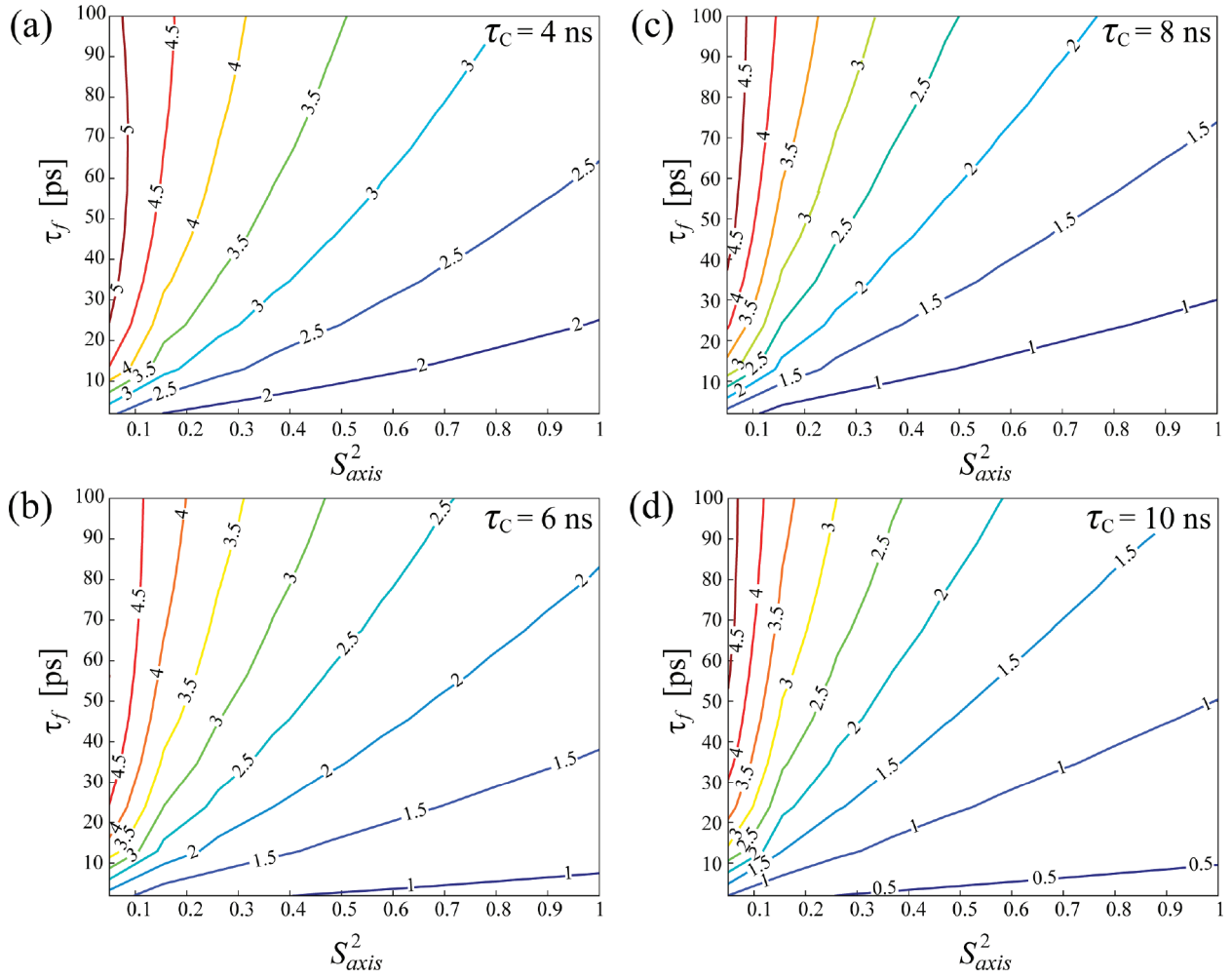

Figure 4. Contour plots showing relative deviations (in %) of the simulated $R_2(CHD_2)$ rates from the $R(D_+,CH_2D)$ rates ($100[R_2(CHD_2) - R(D_+,CH_2D)]/R(D_+,CH_2D)$) as a function of motional parameters (S^2_{axis}; τ_f) for the global molecular reorientation correlation times (τ_C) of (a) 4 ns, (b) 6 ns, (c) 8 ns, and (d) 10 ns. Errors (in %) are indicated for each contour line.

where

$$\rho^{3Q}_{1-4} + \rho^{3Q}_{2-5} \equiv 0.25(D^2_{\pm,1}D_{\pm,2} + D_{\pm,1}D^2_{\pm,2})$$

$$\rho^{3Q}_{1-4} - \rho^{3Q}_{2-5} \equiv 0.25D^2_{\pm,1}(D_{\pm,2}D_{Z,2} + D_{Z,2}D_{\pm,2}) + 0.25D^2_{\pm,2}(D_{\pm,1}D_{Z,1} + D_{Z,1}D_{\pm,1})$$

$$\rho^{4Q}_{1-5} \equiv 0.25(D^2_{\pm,1}D^2_{\pm,2})$$

Therefore, the quadrupolar rates $R_{3Q}(CHD_2)$ and $R_{4Q}(CHD_2)$ are single-exponential and given by

$$R_{3Q}(CHD_2) = \left(\frac{1}{80}\right)(2\pi QCC)^2[9J^A(0) + 21J^A(\omega_D) + 12J^C(\omega_D) + 18J^A(2\omega_D)] \quad (8)$$

$$R_{4Q}(CHD_2) = \left(\frac{3}{40}\right)(2\pi QCC)^2[2J^A(\omega_D) + 4J^A(2\omega_D)] \quad (9)$$

where the auto- and cross-correlation spectral density functions, $J^A(\omega)$ and $J^C(\omega)$, are defined as in eq 2. Finally, the autorelaxation rate of the (nearly) single-exponential longitudinal mode R_L (measured in the experiment of Figure 1, inset B) has been shown earlier to be given by $(3/40)(2\pi QCC)^2[4J(\omega_D) + 4J(2\omega_D)]$.[32]

Relative Sensitivities of Deuterium Relaxation Rate Measurements. Direct comparison of experimental sensitivities in ^2H relaxation rate measurements between the two isotopomers is problematic in view of (i) slightly different content of $^{13}CH_2D$ and $^{13}CHD_2$ isotopomers in the NMR sample, (ii) slower longitudinal relaxation of protons in $^{13}CHD_2$ methyl groups[18,73] necessitating the use of longer recovery delays in $^{13}CHD_2$-directed experiments, and (iii) different efficiencies of the sensitivity-enhancement scheme employed in Figure 1 for $^{13}CH_2(D)$ and $^{13}CH(D_2)$ groups.[46] Therefore, we restrict this analysis to approximate comparison of signal-to-noise ratios obtained in NMR spectra recorded on each individual isotopomer. It is important to keep in mind, however, that the maximum amount of magnetization that can be transferred to deuterons and back is 1/2 in $^{13}CHD_2$ methyls versus 2/3 in their $^{13}CH_2D$ counterparts.[18,19]

In $^{13}CH_2D$ methyl groups, the measurements of rank-2 elements ($D_+D_Z + D_ZD_+$, $3D^2_Z - 2$, D^2_+) are on average 2−2.2-fold less sensitive than the measurement of rank-1 terms (D_+, D_Z). This factor, which is almost temperature-independent (at least within the range of 10−40 °C in ubiquitin), is in agreement with

dx.doi.org/10.1021/jp209304c | J. Phys. Chem. B 2012, 116, 606–620

the previous observations of Millet et al.,[16] and stems exclusively from fast deuterium spin flips during the twice longer $2T_C$ delays needed to transfer the magnetization from ^{13}C nuclei to deuterons and back in rank-2 measurements (Figure 1).

In $^{13}CHD_2$ methyls, the measurements of longitudinal decay, $R_L(CHD_2)$, are on average 2-fold less sensitive than $R_2(CHD_2)$ data sets for the same reason, i.e., twice longer delays $2T_C$: $1/(6J_{CD})$ in $R_2(CHD_2)$ versus $1/(3J_{CD})$ in $R_L(CHD_2)$ experiments (Figure 1) with fast deuterium spin flips attenuating carbon magnetization in the $^{13}C(H)D_2$ pentet on the way to and from ^2H. Note that the net transfer functions in $R_2(CHD_2)$ and $R_L(CHD_2)$ measurements are the same, and at their maxima they "transfer" 1/2 of the magnetization to ^2H and back.

The situation is slightly more complicated with $R_{3Q}(CHD_2)$ and $R_{4Q}(CHD_2)$ experiments. The net transfer functions of the out-and-back process for 3Q and 4Q ^2H rate measurements can be shown to be equal to $[0.5\sin(8\pi J_{CD}T_C) - \sin(4\pi J_{CD}T_C)]^2$ and $(1/8)[1.5 + 0.5\cos(8\pi J_{CD}T_C) - 2\cos(4\pi J_{CD}T_C)]^2$, respectively, with their respective maxima at $T_C = 1/(6J_{CD})$ and $T_C = 1/(4J_{CD})$. These functions transfer maximum 3/16 and 2/9 of magnetization to ^2H and back in $R_{3Q}(CHD_2)$ and $R_{4Q}(CHD_2)$ experiments, respectively. Therefore, in the absence of ^{13}C relaxation, $R_{3Q}(CHD_2)$ and $R_{4Q}(CHD_2)$ data sets are predicted to be (8/3)- and (9/4)-fold less sensitive than the $R_2(CHD_2)$ experiments. In practice, however, fast deuterium spin-flips and differential relaxation of the five lines in the $^{13}CD_2$ group[74,75] during delays $2T_C$ lead to 6−7-fold and almost 10-fold average attenuations of signal-to-noise in the $R_{3Q}(CHD_2)$ and $R_{4Q}(CHD_2)$ measurements compared to $R_2(CHD_2)$. Clearly, $R_{3Q}(CHD_2)$ and $R_{4Q}(CHD_2)$ experiments are very insensitive, resulting in large average standard errors in the extracted relaxation rates—3% and 5% for $R_{3Q}(CHD_2)$ and $R_{4Q}(CHD_2)$, respectively—even after prolonged acquisition times (see Materials and Methods section). $R_{3Q}(CHD_2)$ and $R_{4Q}(CHD_2)$ are therefore interpreted only semiquantitatively in what follows, keeping in mind large uncertainties in the extracted rates. On the other hand, we estimate that $R_2(CHD_2)$ experiments are approximately as sensitive as rank-1 measurements in $^{13}CH_2D$ methyls for the sample of ubiquitin used in this study.

Consistency Relations for ^2H Rates between $^{13}CH_2D$ and $^{13}CHD_2$ Probes. One of the main advantages of ^2H spin relaxation lies in the possibility to verify the consistency of the measured rates prior to analysis in terms of motional parameters.[16,20] Jacobsen and co-workers have shown that in spin systems with a single deuteron (such as $^{13}CH_2D$ methyls or D^α sites in proteins) the following inequalities must hold:[52] $(5/3)R(D_+D_Z + D_ZD_+) \geq R(D_+) \geq (5/3)R(3D_Z^2 - 2) \geq (5/3)R(D_+^2) \geq R(D_Z)$ so long as $J(0) \geq J(\omega_D) \geq J(2\omega_D)$. A more stringent test is if the data satisfies the following "consistency" relations:[52] $R(D_+D_Z + D_ZD_+) = R(D_+) - (2/3)R(3D_Z^2 - 2)$ and $R(D_+^2) = (1/2)R(D_Z) + (1/6)R(3D_Z^2 - 2)$. Figure S1 of the Supporting Information shows that these inequalities and consistency relations are indeed satisfied for ^2H relaxation rates in the studied subset of $^{13}CH_2D$ methyls of ubiquitin at 27 °C. Consistencies between ^2H rates of similar quality have been obtained for $^{13}CH_2D$ methyls at the other two temperatures.

As ^2H relaxation rates in both methyl isotopomers are expressed through linear combinations of the spectral density function $J(\omega)$ evaluated at the same set of frequencies (0, ω_D, and $2\omega_D$), it is more interesting to establish "inter-relationships" between the ^2H rates measured in the two different methyl groups, $^{13}CHD_2$ and $^{13}CH_2D$. One such relation has been established earlier for the relaxation rate R_L of the longitudinal magnetization mode $\{D_{z,1} + D_{z,2} - (3/2)(D_{z,1}D_{z,2}^2 + D_{z,2}D_{z,1}^2)\}$ in $^{13}CHD_2$ methyls:[32]

$$R_L(CHD_2) = R(D_Z; CH_2D) + R(3D_Z^2 - 2; CH_2D) \quad (10)$$

Another relation follows immediately from comparison of eq 1e and eq 9: R_{4Q} rates in $^{13}CHD_2$ groups should be equal to double the relaxation rates of D_+^2 in $^{13}CH_2D$ methyls:

$$R_{4Q}(CHD_2) \approx 2R(D_+^2; CH_2D) \quad (11)$$

The approximate nature of the relation in eq 11 stems from "contamination" of the rates $R(D_+^2;CH_2D)$ and $R_{4Q}(CHD_2)$ due to contributions from dipolar interactions of methyl deuterons with ^{13}C and ^1H spins within the methyl group as well as dipolar interactions with external ^1H spins.[16] These dipolar contributions are partially offset by the nonexponentiality of the decay due to evolution of J_{CD} coupling(s) during the relaxation delay T.[16] A detailed account of how $R(D_+^2;CH_2D)$ rates may be corrected to extract purely quadrupolar contributions has been given by Millet et al.[16] We note that *relative* dipolar contributions to $R(D_+^2;CH_2D)$ and $R_{4Q}(CHD_2)$ decay rates are expected to be different. For example, dipolar interactions between the two deuterons in a $^{13}CHD_2$ group and ^{13}C and ^1H spins will be correlated. These dipole−dipole cross correlations can be shown to be close in magnitude to the autorelaxation terms. Such cross-correlation terms (and especially those involving external proton spins) are difficult to take into account accurately. Considering these difficulties in interpretation of $R_{4Q}(CHD_2)$ rates and the very low sensitivity of their measurements (see above), we have chosen not to include $R_{4Q}(CHD_2)$ in any subsequent analysis in terms of motional parameters. Likewise, the $R(D_+^2;CH_2D)$ rates were used only to establish their approximate consistency with $R_{4Q}(CHD_2)$ according to eq 11.

The third relation concerns $R_{3Q}(CHD_2)$ rates and is exact only in the limit when $J^C(\omega) = J^A(\omega)$ in the expression for spectral density function in eq 2a (i.e., if $\tau_f \rightarrow 0$). In this limit, it follows from eqs 1a,1b, 1d,1e and the expression for $R_{3Q}(CHD_2)$ in eq 8 that $R_{3Q}(CH_2D) = R(D_Z;CH_2D) + R(D_+;CH_2D) + R(3D_Z^2 - 2;CH_2D) - R(D_+^2;CH_2D)$. However, the assumption of $\tau_f \rightarrow 0$ does not hold in practice for any of the studied residues in ubiquitin except for Met1$^\varepsilon$ methyl group at 40 °C. Therefore, a more realistic consistency test that takes into account fast methyl motions ($\tau_f > 0$) would satisfy

$$R_{3Q}(CHD_2) \leq R(D_Z; CH_2D) + R(D_+; CH_2D) + R(3D_Z^2 - 2; CH_2D) - R(D_+^2; CH_2D) \quad (12)$$

Interestingly, for the form of spectral density function in eq 2a, the difference between the rates $R(D_Z) + R(D_+) + R(3D_Z^2 - 2) - R(D_+^2) - R_{3Q}$ is predicted to be independent of global correlation time $\tau_{c,eff}$ as well as S^2_{axis}, and is a function of the time scale of local methyl motions (τ_f) only. Nevertheless, attempts to extract reliable values of τ_f from this difference using the assumed form of the spectral density function did not provide τ_f estimates that would be consistent with those obtained from other analyses.

Figure 5 shows that the above relations between ^2H rates measured in $^{13}CHD_2$ and $^{13}CH_2D$ methyls (eqs 10−12) indeed hold for the studied subset of methyls in ubiquitin at 27 °C. Figures S2 and S3 of the Supporting Information demonstrate that this is also invariably the case at the two other temperatures.

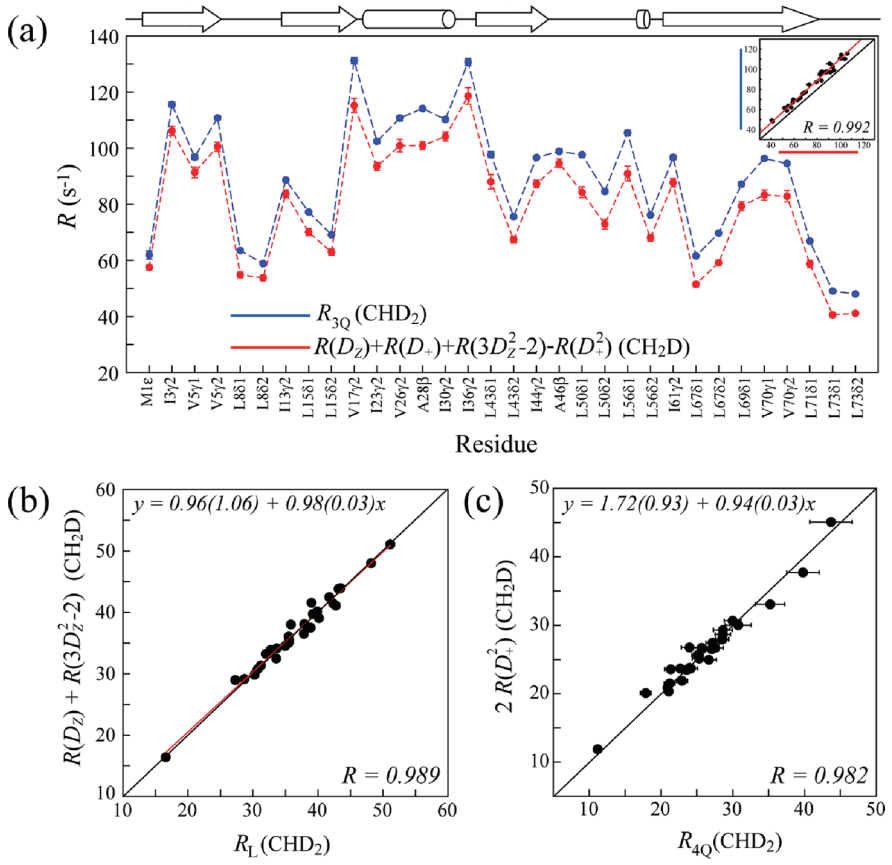

Figure 5. (a) All ^{2}H relaxation rates measured in $^{13}CHD_2$ groups of ubiquitin at 27 °C satisfy the consistency relations. (a) $R_{3Q}(CHD_2) < R(D_Z) + R(D_+) + R(3D_Z^2 - 2) - R(D_+^2)(CH_2D)$ (shown with red and blue circles/lines, respectively vs methyl position). The inset in (a) shows the correlation plot of $R_{3Q}(CHD_2)$ vs $R(D_Z) + R(D_+) + R(3D_Z^2 - 2) - R(D_+^2)(CH_2D)$. (b,c) Linear correlation plots of (b) $R_L(CHD_2)$ rates (*x*-axis) vs $R(D_Z) + R(3D_Z^2 - 2)(CH_2D)$ (*y*-axis), and (c) $R_{4Q}(CHD_2)$ (*x*-axis) vs $2R(D_+;CH_2D)$ (*y*-axis) for 32 methyls of ubiquitin. Schematic representation of the secondary structure of ubiquitin is shown on top of panel (a).

Since relative dipolar contributions to $R(D_+^2;CH_2D)$ rates in eq 12 will increase with $\tau_{c,eff}$, we predict that for significantly larger proteins the relation in eq 12 (Figure 5a, and Figures S2a and S3a of the Supporting Information) will be violated unless the $R(D_+^2;CH_2D)$ rates are corrected appropriately.[16] We note that despite that dipolar contributions to the measured $R_{4Q}(CHD_2)$ and $R(D_+^2;CH_2D)$ rates are predicted to be different as described above, the correlations between $R_{4Q}(CHD_2)$ and $2R(D_+;CH_2D)$ (eq 10) remain very high at all temperatures (Figure 5c, and Figures S2c and S3c of the Supporting Information).

Comparison of $^{13}CH_2D$- and $^{13}CHD_2$-Derived Measures of Order in Methyls of Ubiquitin. As it can be expected from the simulations of $R_2(CHD_2)$ decays described above and the previous work that probed the validity of $R_L(CHD_2)$ as a measure of the time scales of methyl motions,[32] the combination of $R_2(CHD_2)$ and $R_L(CHD_2)$ rates should serve as a measure of methyl-bearing side-chain dynamics that is reliable to within a few percent. In what follows, we compare the motional parameters of methyl dynamics in ubiquitin that are derived from $R(D_+)$, $R(D_Z)$ rates in CH_2D methyls with those obtained from $R_2(R_{3Q})$ and R_L rates in $^{13}CHD_2$ groups. In all analyses, the $R_2(CHD_2)$ and $R_L(CHD_2)$ rates have been best-fit to the expressions for $R(D_+)$ (eq 1a) and $(3/40)(2\pi QCC)^2[4J(\omega_D) + 4J(2\omega_D)]$, respectively. Figure 6 shows linear correlation plots of $[R_L,R_2(CHD_2)]$-derived $(S^2_{axis};\tau_f)$ versus $[R(D_+,D_Z;CH_2D)]$-derived $(S^2_{axis};\tau_f)$ at 10, 27, and 40 °C. Although the correlations of S^2_{axis} are extremely high at all temperatures (Pearson $R \geq 0.997$), a noticeable systematic overestimation of S^2_{axis} derived from the $[R_L,R_2(CHD_2)]$ rates is apparent at 27 and 40 °C (Figure 6b,c). This is the direct consequence of the (slightly) higher $R_2(CHD_2)$ rates as simulated and verified experimentally above: $R_2(CHD_2) > R(D_+;CH_2D)$. Correlations of comparable quality are obtained for the time scales of methyl dynamics (τ_f) derived from the relaxation data acquired on the two methyl isotopomers (Figure 6d–f).

Because of the fast rotation of a methyl group compared to the rate of global molecular tumbling, even in small proteins S^2_{axis} values are primarily determined by transverse relaxation rates (R_2), whereas the time scale of motions (τ_f) predominantly derive from longitudinal relaxation. This separation allows for estimation of errors in $R_2(CHD_2)$-derived S^2_{axis} neglecting (to a good approximation) the contributions to S^2_{axis} from $R_L(CHD_2)$. Generation of synthetic $[R_2, R_L(CHD_2)]$ data sets as a function of $(S^2_{axis};\tau_f)$ parameters using full relaxation matrices for $R_2(CHD_2)$ rates (see Supporting Information) and back-fitting the synthetic data to extract $(S^2_{axis};\tau_f)$ allowed us to simulate absolute deviations of $[R_L,R_2(CHD_2)]$-derived S^2_{axis} from the "input" S^2_{axis} values. Figure S4 of the Supporting Information shows the contour plots of absolute differences between such synthetic-$(R_2;R_L)$-derived and "input" S^2_{axis} values, $S^2_{axis}(CHD_2) - S^2_{axis}$, as a function of $(S^2_{axis};\tau_f)$ for τ_C values of 4 ns (Figure S4a) and 10 ns (Figure S4b). These deviations arise exclusively from fitting of the $R_2(CHD_2)$ rates to the "wrong" expression for the relaxation rate—namely, that of $R(D_+;CH_2D)$ in eq 1a. The predicted absolute

dx.doi.org/10.1021/jp209304c |J. Phys. Chem. B 2012, 116, 606–620

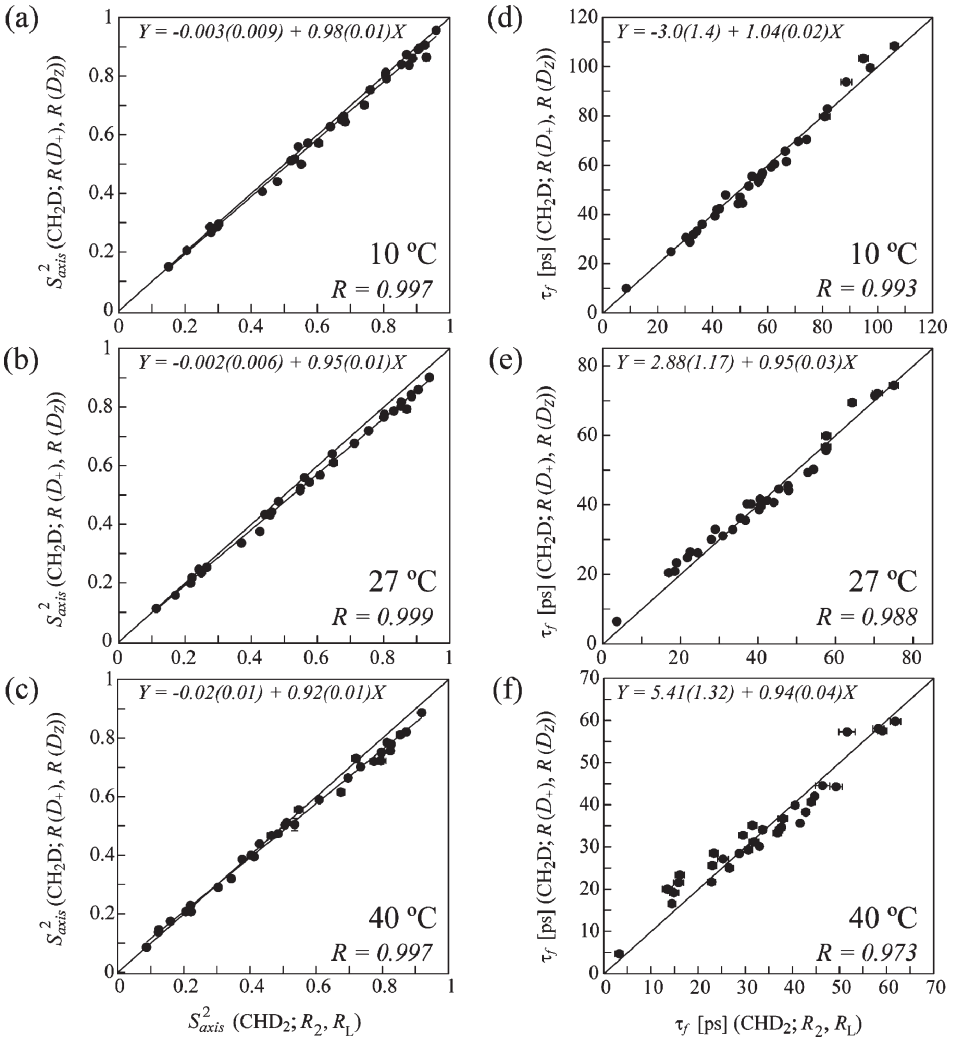

Figure 6. Linear correlation plots of (a−c) $[R_2,R_L(CHD_2)]$-derived S^2_{axis} (x-axis) vs $[R(D_+,D_Z;CH_2D)]$-derived S^2_{axis} (y-axis) at 10, 27, and 40 °C; (d−f) $[R_2,R_L(CHD_2)]$-derived τ_f values (x-axis) vs $[R(D_+,D_Z;CH_2D)]$-derived τ_f (y-axis) at 10, 27, and 40 °C. Linear regression parameters are shown for each plot along with Pearson correlation coefficient, R. Solid diagonal lines correspond to $y = x$.

errors in S^2_{axis} are small and invariably positive for both τ_C values. Nevertheless, for a small protein with $\tau_C < \sim 10$ ns, the errors in S^2_{axis} corresponding to the average dynamics parameters in ubiquitin (in the range between 0.025 and 0.035; Figure S4a) are likely to be higher than random errors in S^2_{axis} determination. The plots in Figure S4a predict that for the same value of τ_f absolute errors in $R_2(CHD_2)$-derived S^2_{axis} increase slightly for higher order parameters. This qualitatively explains why the slopes different from unity are obtained in the linear regression analyses in Figure 5a−c. On average, the simulated absolute errors in S^2_{axis} agree with the differences between $[(R_2,R_L;CHD_2)]$-derived and $[R_2(D_+,D_Z;CH_2D)]$-derived S^2_{axis}. Figure S5 in the Supporting Information shows the differences between the $[(R_2,R_L;CHD_2)]$-derived and $[(D_+,D_Z;CH_2D)]$-derived S^2_{axis} values in ubiquitin at 40 °C plotted against residue numbers. From the linear regression parameters of the correlations in Figure 5a−c, we find empirically that uniform correction factors of 0.95(0.89) for $[(R_2,R_L;CHD_2)]$-derived S^2_{axis} of ubiquitin at 27(40 °C) (corresponding τ_C values of 5.0 and 3.6 ns) are suitable for all practical purposes. Alternatively, the $R_2(CHD_2)$ rates can be scaled on a grid of $(S^2_{axis};\tau_f)$ parameters according to Figure 4. In this case, initial estimates of $(S^2_{axis};\tau_f)$ can be determined from the "raw" (uncorrected) $R_2(CHD_2)$ rates. Both correction procedures lead to practically identical results as far as the resulting motional parameters of side-chain dynamics are concerned.

An additional verification that the errors in $[(R_2,R_L;CHD_2)]$-derived S^2_{axis} arise from slight nonexponentiality of $R_2(CHD_2)$ decays and their subsequent interpretation as if these rates were single-exponential and equal to $R(D_+;CH_2D)$, is provided by extracting the dynamics parameters $(S^2_{axis};\tau_f)$ from the combination of $R_{3Q}(CHD_2)$ and $R_L(CHD_2)$ rates. Figure S6 of the Supporting Information shows linear correlation plots of $[(R_{3Q},R_L;CHD_2)]$-derived and $[R(D_+,D_Z;CH_2D)]$-derived S^2_{axis} and τ_f at 10, 27, and 40 °C. The correlations between the two sets of motional parameters remain high (Pearson $R > 0.97$) despite that the errors in S^2_{axis} are very substantial arising from much poorer sensitivity of $R_{3Q}(CHD_2)$ relaxation rate measurements. Importantly though, the systematic deviations between the S^2_{axis} values obtained in the two isotopomers apparent in Figure 6b,c are eliminated in the plots of Figure S6b,c. We note that all the correlations of $R(CHD_2)$-derived dynamics parameters have been made with their counterparts obtained from rank-1 rates in $^{13}CH_2D$ methyls. Correlations of very similar quality are obtained if rank-2

dx.doi.org/10.1021/jp209304c |J. Phys. Chem. B 2012, 116, 606–620

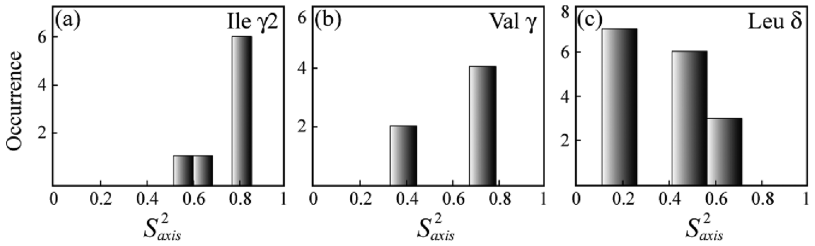

Figure 7. Distributions of $(R_2,R_L;CHD_2)$-derived S^2_{axis} for (a) Ile$^{\gamma 2}$, (b) Val$^{\gamma}$, and (c) Leu$^{\delta}$ methyls of ubiquitin.

rates in $^{13}CHD_2$ groups are used instead. It is also noteworthy that ^{13}C relaxation during the two $2T_C$ periods in the experiment of Figure 1 has been neglected in the analysis of errors associated with the measurement and interpretation of $R_2(CHD_2)$ rates in small (τ_C < 10 ns) proteins presented above. Differential relaxation of the lines of the $^{13}CD_2$ pentet can introduce additional sources of errors.[74,75] Taking into account the differential decay rates of these lines under the effect of quadrupolar and dipolar spin interactions shows that their effect on the out-and-back transfer of the combination of ^2H coherences in expression 5 is small but may partially account for somewhat larger experimental differences between $[(R_L,R_2;CHD_2)]$-derived and $[R(D_+,D_Z;CH_2D)]$-derived S^2_{axis} (Figure 6b,c and Figure S5, Supporting Information) compared to those predicted from simulations (Figure S4, Supporting Information).

^{2}H-Derived Dynamics Parameters of Methyl-Containing Side Chains in Ubiquitin. Comparisons with MD Simulations. Perhaps the most telling test of the reliability of the derived dynamics parameters is their mutual comparison for different temperatures. Such a verification would uncover any problems with relaxation measurements and/or the procedure of $(S^2_{axis};\tau_f)$ derivation from experimental rates. A comparison of methyl $R(D_+,D_Z;CH_2D)$-derived and $[(R_{3Q},R_L;CHD_2)]$-derived motional parameters obtained for 32 methyls of ubiquitin at the three temperatures by fitting the relaxation rates to the simplest form of the spectral density function (eq 2a) is shown in Figure S7 of the Supporting Information. Clearly, S^2_{axis} values decrease at higher temperatures for both sets of data without exceptions (Figure S7a,c); the same trend is evident for the correlation times of local motions in Figure S7b,d, lending confidence in the dynamics parameters of methyl groups derived from both methyl isotopomers.

Residue-specific distributions of $^{13}CHD_2$-derived S^2_{axis} values at 27 °C in ubiquitin are shown as histograms in Figure 7 after scaling of S^2_{axis} by a uniform factor of 0.95. Although the number of methyl probes of each type is hardly sufficient for reliable statistical analysis of S^2_{axis} distributions, our data are qualitatively consistent with earlier experimental[24,42,76,77] and MD-predicted[39] S^2_{axis} profiles. Specifically, the clear two-pronged distributions of S^2_{axis} for Val$^{\gamma}$ and Ile$^{\gamma 2}$ methyls (Figures 7a,b) result from a distribution of side chains that are either confined to a single state of the dihedral angle χ_1 (higher S^2_{axis}) or undergo jumps between different states (lower S^2_{axis}). In Leu side chains the three-pronged profile (Figure 7c) reflects either (i) both χ_1 and χ_2 having large (>90%) preference for one rotamer (the highest S^2_{axis}); (ii) only χ_1 or χ_2 angles having large preference for one rotamer (medium S^2_{axis}), and (iii) neither χ_1 nor χ_2 having large preferences for a single rotameric state (the lowest S^2_{axis}). Note that S^2_{axis} of methyls further removed from the backbone (Leu$^{\delta}$) are characterized by on average lower ordering than those closer to the backbone as in Val$^{\gamma}$ and Ile$^{\gamma 2}$ methyls. Likewise, Ala$^{\beta}$ methyls are tightly coupled to the backbone and display higher than average S^2_{axis}: 0.90 ± 0.02 in Ala28$^{\beta}$ and 0.82 ± 0.01 in Ala46$^{\beta}$ of ubiquitin at 27 °C.

So far, the dynamics parameters derived from ^2H spin relaxation rates in both methyl isotopomers were considered separately using the simplest form of the model-free spectral density function $J(\omega)$ (eq 2a). It is of interest to establish how these derived measures of order are dependent on the choice of the model for $J(\omega)$. The identification of slower motions of the methyl 3-fold axis on the time scales of several hundreds of picoseconds to a few nanoseconds is notoriously ridden with difficulties and prone to large uncertainties in the derived dynamics parameters.[20,27,61,62] Previously, Choy and Kay[61] unequivocally showed that selection of motional models for methyl-containing side chains from ^2H relaxation data is limited by the low number of frequencies at which $J(\omega)$ is sampled: only three in the case of deuterons: 0, ω_D, $2\omega_D$. This "undersampling" problem is the primary source of large ambiguities in model selection and the uncertainties in dynamics parameters, especially so when ^2H data at only a single spectrometer field are available. Note that the addition of CHD_2 rates that sample $J(\omega)$ at the same three frequencies to the pool of experimental data does not alleviate these difficulties.

We have therefore opted for the most conservative approach possible for the identification of slow side-chain motions choosing to fit the rates from CH_2D and CHD_2 methyls that cannot be expressed as simple linear combinations of each other, namely, four rank-1 and rank-2 CH_2D rates barring the $R(D^2_+)$, i.e., $R(D_+, D_Z,D_+D_Z + D_ZD_+,3D^2_Z - 2)$ and the $R(3Q;CHD_2)$ rates, to the spectral density form in eq 2b.[58] Furthermore, to ensure the stability of the fitting procedure and to reduce the number of free parameters, the order parameters of fast librational methyl motions (S^2_f in eq 2b) were fixed to their residue-specific values obtained from MD simulations: MD-derived S^2_f values in ubiquitin are usually high and do not vary significantly (0.87 ± 0.06). The values of reduced χ^2 obtained from the fits using eqs 2a and 2b were subjected to the *F*-test[78] with 20% confidence limit. Only several methyls of ubiquitin consistently passed the *F*-test at all the three temperatures with well-defined values of the slow motion correlation times (τ_{CC} in eq 2b) in the range between 200 ps and 1.8 ns—Leu8$^{\delta 1,2}$, Ile13$^{\gamma 2}$ in the flexible loop Leu8-Lys11 and the beginning of the second β-strand, as well as Val70$^{\gamma 1,2}$, Leu71$^{\delta 1}$, and Leu73$^{\delta 1,2}$ in the end of the final β-strand and the C-terminus of the protein, indicating high probability of nanosecond motions of the C−C bond (slow rotameric jumps) at these methyl positions. Interestingly, the side chain of Leu8 was previously shown to be involved in correlated dynamics on multiple time scales from relaxation rate measurements of ZQ and DQ coherences in methyl groups.[79] Leu8 together with Ile44 and Val70 form a hydrophobic patch on the surface of ubiquitin

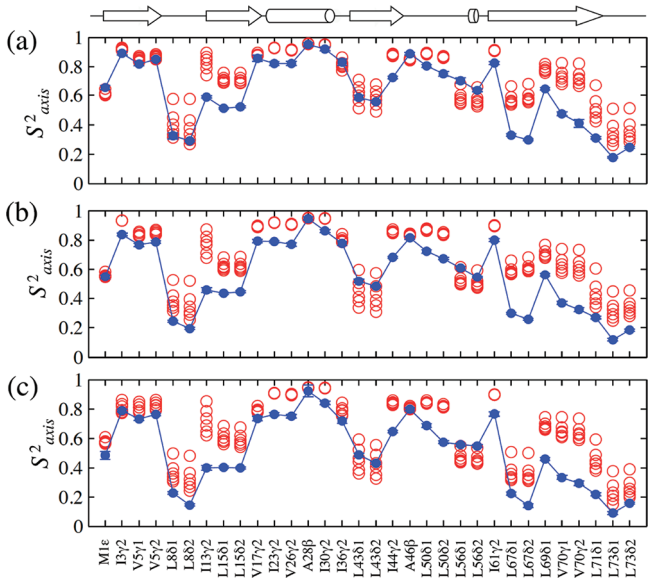

Figure 8. Comparison of the S^2_{axis} values derived from ^{2}H NMR spin relaxation experiments (blue filled circles) and MD simulations (red open circles) at three temperatures (a) 10 °C, (b) 27 °C, and (c) 40 °C, respectively. MD-derived S^2 values are represented by a range of values calculated over consecutive time windows from 1 to 15 ns. Secondary structure elements of ubiquitin are indicated on top of the figure.

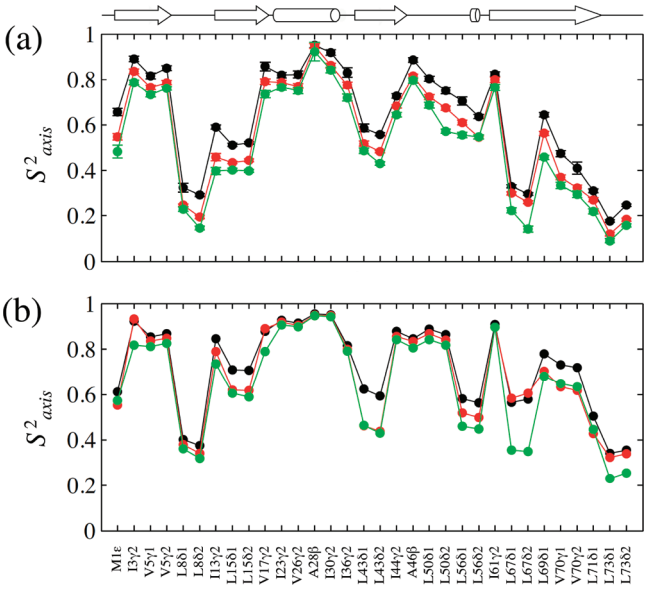

Figure 9. Temperature dependence of S^2_{axis} values determined (a) from ^{2}H NMR spin relaxation experiments and (b) from MD trajectories (averaged over consecutive 5 ns time windows). The color coding represents temperatures at 10 °C (black), 27 °C (red), and 40 °C (green), respectively. Secondary structure elements of ubiquitin are indicated on top of the figure.

that is essential for binding to the ubiquitin-activating enzyme E1.[80−82]

Figure 8 shows a comparison of thus derived S^2_{axis} values (S^2_{CC} if the fit to eq 2b passed the 20% *F*-test at all temperatures) obtained for 32 methyl groups of ubiquitin at the three temperatures with their 1 μs MD-derived counterparts. For those methyl groups that show relatively slow internal motions comparable to the overall tumbling correlation time (hundreds of picoseconds to a few nanoseconds), the window size for calculating S^2_{axis} from the MD trajectory will directly affect the calculated values. In the present study, a range of S^2_{MD} values are back-calculated over time windows from 1 to 15 ns for comparison with the experimentally derived S^2_{axis}(S^2_{CC}). The spread of S^2_{MD} for a given residue for variable window size in Figure 8 reflects the sensitivity of these values to the precise internal motional time scales. When the time scales of the local and overall motions are well separable ($\tau_{local} \ll \tau_C$), the back-calculated S^2_{MD} values converge to a single point as is the case for some of the more rigid methyl groups. As can be also seen in Figure 8, the majority of methyl groups with low S^2 (<0.5) exhibit slower internal motions, i.e., comparable to the overall tumbling correlation time. Although several individual values of S^2_{axis} are in disagreement between the two sets, the pattern of ^{2}H-relaxation-derived S^2 variations is remarkably well reproduced by MD simulations at all temperatures (Figure 8). The correlation between the two sets of data is high (Pearson $R = 0.89$ for a 5 ns time window) although the force field used to derive in silico S^2 values (see Materials and Methods) slightly overestimates the rigidity of side chains on average. The most conspicuous deviations in S^2 between the two sets can be noted for Ile13$^{\gamma 2}$, Leu15$^{\delta 1,2}$, Leu50$^{\delta 1,2}$, Leu67$^{\delta 1,2}$, Leu69$^{\delta 1}$, and Val70$^{\gamma 1,2}$ methyls. Methyl groups of Leu67$^{\delta 1,2}$ and Leu69$^{\delta 1}$ are a part of a hydrophobic cluster that includes also Leu15$^{\delta 2}$, Leu43$^{\delta 1,2}$, Leu50$^{\delta 1,2}$, Leu56$^{\delta 1,2}$, and Leu71$^{\delta 1,2}$ methyls. It appears that the order parameters of some methyls in this hydrophobic patch can be reproduced by MD simulations with higher fidelity than the others, with Leu67$^{\delta 1,2}$ and to a certain extent Leu15$^{\delta 1,2}$ and Leu69$^{\delta 1}$ showing larger discrepancies (Figure 8). Interestingly, some of the residues with noticeable disagreement between the two sets are apparently involved in slow motions/rotameric jumps according to ^{2}H spin relaxation data: Ile13$^{\gamma 2}$, Val70$^{\gamma 1,2}$, and Leu71$^{\delta 1}$. We note that for low order parameters ($S^2 < \sim 0.5$) the values of S^2 barely depend on the motional model used; i.e., practically the same values of S^2_{axis} (eq 2a) and S^2_{CC} (eq 2b) are obtained to within error margins for Ile13$^{\gamma 2}$, Val70$^{\gamma 1,2}$, and Leu71$^{\delta 1}$ using the fitting procedure for ^{2}H relaxation rates described above.

Temperature dependence of S^2_{axis} values derived from ^{2}H NMR spin relaxation measurements using the fitting procedure described above is illustrated in Figure 9a, while the S^2_{MD} values averaged over 5 ns window at the three different temperatures are compared in Figure 9b. Anticorrelation between temperature and S^2_{axis} is apparent in both sets of data. In the MD simulations, however, the temperature dependence of the order parameters of residues belonging to regular secondary structural elements (indicated at the top of the figure) is somewhat less pronounced than in the experiment (cf. Figure 9, a and b). This trend is especially noticeable in the α-helix of ubiquitin (residues Ile23-Glu34) as well as the methyls of Ala46$^{\beta}$ and Leu50$^{\delta 1,2}$. The temperature dependence of experimental S^2_{axis} is conspicuously more uniform throughout the protein sequence and is largely independent of secondary structure (Figure 9). Considering that the dynamics of methyl-containing side chains is not necessarily correlated with that of the protein backbone,[83,84] we note that the temperature dependence of side-chain ordering may reflect slight changes in the packing of the hydrophobic core of the protein rather than changes in association of the secondary structure elements (e.g., weaker hydrogen bonding at higher temperatures). The temperature dependence of the time scales of slow methyl axis motions/rotameric jumps (τ_{CC}) for the subset of

methyl groups of ubiquitin that have statistically significant reduction in the reduced χ^2 when five ^{2}H relaxation rates, $R(D_+,D_Z,D_+D_Z + D_ZD_+,3D_Z^2 - 2;CH_2D)$ and $R(3Q;CHD_2)$, are best-fit to the spectral density function in eq 2b is illustrated in Figure S8 of the Supporting Information. Although most τ_{CC} values are ill-defined, the temperature dependence in Figure S8 is (to within errors) consistent with the expectation that rotameric reorientation of side chains slows down at lower temperatures.

A detailed study of the temperature dependence of backbone amide and methyl order parameters in ubiquitin was conducted previously and included the testing for anharmonicity of the underlying motions.[85] Using the parameter describing the (an)-harmonicity of the potential energy function, $\Lambda = d\ln(1 - S^2_{axis})/d\ln T$,[86] where T is temperature in kelvin ($\Lambda \leq 1$ for a simple harmonic oscillator) the authors showed that on average the Λ values significantly exceed 1 for backbone amides (7.1 ± 2.6) but are much lower for methyl groups of ubiquitin (2.26 ± 1.0).[85] For the subset of methyl groups and the temperature range used in the present work, the average MD-derived value of Λ is 3.1 ± 2.1 that compares well with the average experimental Λ of 3.2 ± 2.2. Of note, numerous methyls show in the simulations a significant temperature dependence of their Λ values and in some cases they even change sign, which was also observed by Wand and co-workers.[85]

Earlier, Lee et al.[42] presented a detailed analysis of ^{2}H- and ^{13}C-relaxation derived motional characteristics of methyl groups in ubiquitin at 30 °C. Although ^{2}H-derived S^2_{axis} values reported in this study are systematically higher than those obtained in the present work at 27 °C (by 14% on average with a high correlation between the two sets, Pearson $R = 0.98$), the lowest order parameters—such as for Leu8$^{\delta1,2}$, Ile13$^{\gamma2}$ and Leu67$^{\delta1,2}$, Leu69$^{\delta1}$ positions—are in very good agreement with the present data: S^2_{axis} of $0.23 \pm 0.01(0.21 \pm 0.01)$ versus $0.27 \pm 0.02(0.21 \pm 0.02)$ reported by Lee et al.[42] for Leu8$^{\delta1}$(Leu8$^{\delta2}$) methyls; 0.54 ± 0.02 versus 0.56 ± 0.03 for Ile13$^{\gamma2}$; $0.25 \pm 0.01(0.30 \pm 0.03)$ versus $0.23 \pm 0.02(0.29 \pm 0.03)$ for Leu67$^{\delta1}$(Leu67$^{\delta2}$) sites, and 0.57 ± 0.02 versus 0.55 ± 0.05 for Ile69$^{\delta1}$. A good agreement can also be noted for this subset of methyl positions with residual dipolar couplings (RDC)-derived S^2_{axis} in ubiquitin by Griesinger and co-workers, even though RDCs measured in multiple alignment media report on a much wider range of time scales from nanoseconds to microseconds.[87]

CONCLUDING REMARKS

In summary, we demonstrated the feasibility of the measurement of a total of nine deuterium spin relaxation rates in $^{13}CH_2D$ and $^{13}CHD_2$ methyl isotopomers of small proteins. In addition to five measurable ^{2}H relaxation rates of D_+, D_Z, $D_+D_Z + D_ZD_+$, $3D_Z^2 - 2$, and D_+^2 elements in a single-deuteron $^{13}CH_2D$ methyl group,[16] the measurement of additional four rates of single-exponentially or nearly single-exponentially decaying magnetization terms in methyls of the $^{13}CHD_2$ variety is described: transverse relaxation rate R_2, longitudinal rate R_L, and the rates of higher order ^{2}H coherences, R_{3Q} and R_{4Q}. Using rigorous analysis of ^{2}H spin relaxation in fast-rotating ($^{13}CH)D_2$ spin systems containing two equivalent deuterons, we derived "consistency" relationships between ^{2}H relaxation rates measured in isotopomers of each type and verified them experimentally on a sample of the protein ubiquitin selectively ^{13}C-labeled at Ile$^{\gamma2}$, Val$^{\gamma}$, Leu$^{\delta}$, Ala$^{\beta}$, and Met$^{\varepsilon}$ methyl sites.

A detailed comparison of methyl-bearing side-chain dynamics parameters (S^2_{axis}; τ_f) obtained from relaxation measurements in $^{13}CH_2D$ and $^{13}CHD_2$ methyls of ubiquitin at 10, 27, and 40 °C reveals that ^{2}H relaxation rates in $^{13}CHD_2$ methyls are reliable and accurate reporters of the amplitudes of methyl 3-fold axis motions (S^2_{axis}) for protein molecules with global molecular tumbling times $\tau_C > \sim 9$ ns. For smaller molecules, a slight correction of the $R_2(CHD_2)$ rates or, alternatively, of the $^{13}CHD_2$-derived S^2_{axis} values is shown to be sufficient for most practical purposes. The values of $^{13}CHD_2$- and $^{13}CHD_2$-derived S^2_{axis} in ubiquitin are in good agreement with those obtained from 1 μs long MD simulations in explicit solvent at all temperatures except for a couple of methyl sites, while the side-chain-specific S^2_{axis} distributions confirm their relation to the side-chain rotameric state preferences predicted from earlier MD simulations.

Whereas deuterons in $^{13}CHD_2$ methyls have been used as quantitative probes of side-chain mobility via the measurements of R_2 and R_L rates in much larger proteins in a number of previous studies,[7,9,18,32−34] the present work represents the first thorough assessment of the validity of ^{2}H probes of dynamics in $^{13}CHD_2$ methyls of smaller molecules where the contributions of high-frequency components to (generally non-single-exponential) decay rates are small but noticeable. For sensitivity reasons, the measurement of relaxation rates of higher order ^{2}H terms, R_{3Q} and especially R_{4Q}, are likely to be limited to relatively small and well-behaved protein molecules in the foreseeable future. Nevertheless, using a cryogenically cooled probe, we have been able to measure the R_{3Q} rates in a 0.8 mM [U-^{2}H; Ala$^{\beta}$-$^{13}CHD_2$]-labeled sample of an 82 kDa enzyme Malate Synthase G (MSG)[88,89] at 37 °C within a reasonable amount of acquisition time (~2 days for the relaxation series). Not surprisingly, because the contributions of the spectral density function evaluated at high frequencies (ω_D and $2\omega_D$) to transverse relaxation rates are negligible in large proteins, the obtained R_{3Q} rates in MSG are the same as $R_2(CHD_2)$ rates to within experimental uncertainties (~4−5%).

Among the nine (nearly) single-exponential ^{2}H spin relaxation rates in the two methyl isotopomers, the measurements of (R_2, R_1) in $^{13}CH_2D$ groups, and (R_2, R_L) in $^{13}CHD_2$ methyls are the most sensitive and therefore preferred for practical applications. Because of inherently lower sensitivity of the remaining five rate measurements (three rank-2 rates in $^{13}CH_2D$, and R_{3Q}, R_{4Q} in $^{13}CHD_2$ methyls), they are likely to be of practical use primarily for validation purposes using the consistency relationships derived earlier[16,32,52] as well as in the present work. It is also noteworthy that the availability of $^{13}CHD_2$ probes allows for a comparison of ^{2}H-derived dynamics parameters with those obtained from ^{13}C spin relaxation studies as it has been demonstrated previously on a number of protein systems.[7,23,33,42] The interpretation of ^{13}C methyl relaxation rates in terms of side-chain dynamics parameters is generally less straightforward and hence more error prone, a disadvantage which is partially offset by a factor of 2−5 higher sensitivity of ^{13}C relaxation measurements.[7,9,23,33,42]

ASSOCIATED CONTENT

Supporting Information. One figure showing the plots of consistency relationships between the five ^{2}H relaxation rates measured in $^{13}CH_2D$ methyl groups of ubiquitin at 27 °C. Two figures showing the plots of consistency relationships between ^{2}H relaxation rates measured in $^{13}CHD_2$ and $^{13}CH_2D$ methyls of ubiquitin at 10 and 40 °C. One figure showing simulated absolute differences between synthetic-[R_L; $R_2(CHD_2)$]-derived and

input S^2_{axis} values ($S^2_{axis}(CHD_2) - S^2_{axis}$) as a function of ($S^2_{axis}$; τ_f) for the global isotropic molecular reorientation correlation times of 4 and 10 ns. One figure showing absolute differences between the [R_2, $R_L(CHD_2)$]-derived and [D_+, $D_Z(CH_2D)$]-derived methyl S^2_{axis} values in ubiquitin at 40 °C. One figure showing linear correlation plots of [R_{3Q}, $R_L(CHD_2)$]-derived versus [$R(D_+,D_Z; CH_2D)$]-derived (S^2_{axis}; τ_f) at 10, 27, and 40 °C. One figure showing comparisons of (S^2_{axis}; τ_f) values obtained for 32 methyl groups of ubiquitin at 10, 27, and 40 °C. One figure showing the temperature dependence of the time scales of slow rotameric jumps (τ_{CC}) in a subset of methyl groups in ubiquitin. Also provided are the details of simulations of $R_2(CHD_2)$ decay. This material is available free of charge via the Internet at http://pubs.acs.org.

AUTHOR INFORMATION

Corresponding Author

*E-mail: vitali@umd.edu. Tel: ++1-301-4051504. Fax: ++1-301-3140386.

Note

[§]X.L. is on leave from the Department of Chemistry, Xiamen University, China.

ACKNOWLEDGMENT

The authors thank Dr. Chenyun Guo (University of Maryland) for preparation of the [3-$^{13}C_1$]-pyruvate-derived sample of human ubiquitin, and Prof. Lewis E. Kay (University of Toronto, Canada) for stimulating discussions. This work was supported by the National Science Foundation (grant MCB-0918362) to R.B.

REFERENCES

(1) Karplus, M.; McCammon, J. A. *Annu. Rev. Biochem.* **1983**, *53*, 263–300.
(2) Karplus, M.; Kuriyan, J. *Proc. Natl. Acad. Sci. U.S.A.* **2005**, *102*, 6679–6685.
(3) Kern, D.; Zuiderweg, E. R. *Curr. Opin. Struct. Biol.* **2003**, *13*, 748–757.
(4) Tzeng, S. R.; Kalodimos, C. G. *Nature* **2009**, *462*, 368–372.
(5) Tzeng, S. R.; Kalodimos, C. G. *Curr. Opin. Struct. Biol.* **2011**, *21*, 62–67.
(6) Frederick, K. K.; Marlow, M. S.; Valentine, K. G.; Wand, A. J. *Nature* **2007**, *448*, 325–329.
(7) Tugarinov, V.; Kay, L. E. *Biochemistry* **2005**, *44*, 15970–15977.
(8) Gelis, I.; Bonvin, A. M.; Keramisanou, D.; Koukaki, M.; Gouridis, G.; Karamanou, S.; Economou, A.; Kalodimos, C. G. *Cell* **2007**, *131*, 756–769.
(9) Sprangers, R.; Kay, L. E. *Nature* **2007**, *445*, 618–622.
(10) Pickett, S. D.; Sternberg, M. J. *J. Mol. Biol.* **1993**, *231*, 825–839.
(11) Akke, M.; Brüschweiler, R.; Palmer, A. G. *J. Am. Chem. Soc.* **1993**, *115*, 9832–9833.
(12) Igumenova, T. I.; Frederick, K. K.; Wand, A. J. *Chem. Rev.* **2006**, *106*, 1672–1699.
(13) Jarymowycz, V. A.; Stone, M. J. *Chem. Rev.* **2006**, *106*, 1624–1671.
(14) Abragam, A. *Principles of Nuclear Magnetism*; Clarendon Press: Oxford, UK, 1961.
(15) Muhandiram, D. R.; Yamazaki, T.; Sykes, B. D.; Kay, L. E. *J. Am. Chem. Soc.* **1995**, *117*, 11536–11544.
(16) Millet, O.; Muhandiram, D. R.; Skrynnikov, N. R.; Kay, L. E. *J. Am. Chem. Soc.* **2002**, *124*, 6439–6448.
(17) Yang, D.; Kay, L. E. *J. Magn. Reson. Ser. B* **1996**, *110*, 213–218.
(18) Tugarinov, V.; Ollerenshaw, J. E.; Kay, L. E. *J. Am. Chem. Soc.* **2005**, *127*, 8214–8225.
(19) Sheppard, D.; Sprangers, R.; Tugarinov, V. *Prog. Nucl. Magn. Reson. Spectrosc.* **2010**, *56*, 1–45.
(20) Skrynnikov, N. R.; Millet, O.; Kay, L. E. *J. Am. Chem. Soc.* **2002**, *124*, 6449–6460.
(21) Kay, L. E.; Muhandiram, D. R.; Wolf, G.; Shoelson, S. E.; Forman-Kay, J. D. *Nat. Struct. Biol.* **1998**, *5*, 156–163.
(22) Ishima, R.; Louis, J. M.; Torchia, D. A. *J. Mol. Biol.* **2001**, *305*, 515–521.
(23) Ishima, R.; Petkova, A. P.; Louis, J. M.; Torchia, D. A. *J. Am. Chem. Soc.* **2001**, *123*, 6164–6171.
(24) Lee, A. L.; Wand, A. J. *Nature* **2001**, *411*, 501–504.
(25) Lee, A. L.; Kinnear, S. A.; Wand, A. J. *Nat. Struct. Biol.* **2000**, *7*, 72–77.
(26) Desjarlais, J. R.; Handel, T. M. *J. Mol. Biol.* **1999**, *290*, 305–318.
(27) Millet, O.; Mittermaier, A.; Baker, D.; Kay, L. E. *J. Mol. Biol.* **2003**, *329*, 551–563.
(28) Yang, D.; Mittermaier, A.; Mok, Y. K.; Kay, L. E. *J. Mol. Biol.* **1998**, *276*, 939–954.
(29) Pervushin, K.; Wider, G.; Wüthrich, K. *J. Am. Chem. Soc.* **1997**, *119*, 3842–3843.
(30) Vold, R. L.; Vold, R. R. *Prog. Nucl. Magn. Reson. Spectrosc.* **1978**, *12*, 79–133.
(31) Vold, R. L.; Vold, R. R.; Poupko, R.; Bodenhausen, G. *J. Magn. Reson.* **1980**, *38*, 141–161.
(32) Tugarinov, V.; Kay, L. E. *J. Am. Chem. Soc.* **2006**, *128*, 12484–12489.
(33) Godoy-Ruiz, R.; Guo, C.; Tugarinov, V. *J. Am. Chem. Soc.* **2010**, *132*, 18340–18350.
(34) Tugarinov, V.; Kay, L. E. *Chembiochem* **2005**, *6*, 1567–1577.
(35) Baldwin, A. J.; Religa, T. L.; Hansen, D. F.; Bouvignies, G.; Kay, L. E. *J. Am. Chem. Soc.* **2010**, *132*, 10992–10995.
(36) Religa, T. L.; Kay, L. E. *J. Biomol. NMR* **2010**, *47*, 163–169.
(37) Otten, R.; Chu, B.; Krewulak, K. D.; Vogel, H. J.; Mulder, F. A. *J. Am. Chem. Soc.* **2010**, *132*, 2952–2960.
(38) Guo, C.; Tugarinov, V. *J. Biomol. NMR* **2010**, *46*, 127–133.
(39) Best, R. B.; Clarke, J.; Karplus, M. *J. Am. Chem. Soc.* **2004**, *126*, 7734–7735.
(40) Rosen, M. K.; Gardner, K. H.; Willis, R. C.; Parris, W. E.; Pawson, T.; Kay, L. E. *J. Mol. Biol.* **1996**, *263*, 627–636.
(41) Lee, A. L.; Urbauer, J. L.; Wand, A. J. *J. Biomol. NMR* **1997**, *9*, 437–440.
(42) Lee, A. L.; Flynn, P. F.; Wand, A. J. *J. Am. Chem. Soc.* **1999**, *121*, 2891–2902.
(43) Lundström, P.; Teilum, K.; Carstensen, T.; Bezsonova, I.; Wiesner, S.; Hansen, D. F.; Religa, T. L.; Akke, M.; Kay, L. E. *J. Biomol. NMR* **2007**, *38*, 199–212.
(44) Lundström, P.; Vallurupalli, P.; Hansen, D. F.; Kay, L. E. *Nat. Protoc.* **2009**, *4*, 1641–1648.
(45) Shaka, A. J.; Keeler, J.; Frenkiel, T.; Freeman, R. *J. Magn. Reson.* **1983**, *52*, 335–338.
(46) Schleucher, J.; Schwendinger, M.; Sattler, M.; Schmidt, P.; Schedletzky, O.; Glaser, S. J.; Sørensen, O. W.; Griesinger, C. *J. Biomol. NMR* **1994**, *4*, 301–306.
(47) Kay, L. E.; Keifer, P.; Saarinen, T. *J. Am. Chem. Soc.* **1992**, *114*, 10663–10665.
(48) Schleucher, J.; Sattler, M.; Griesinger, C. *Angew. Chem., Int. Ed. Engl.* **1993**, *32*, 1489–1491.
(49) Marion, D.; Ikura, M.; Tschudin, R.; Bax, A. *J. Magn. Reson.* **1989**, *85*, 393.
(50) Delaglio, F.; Grzesiek, S.; Vuister, G. W.; Zhu, G.; Pfeifer, J.; Bax, A. *J. Biomol. NMR* **1995**, *6*, 277–293.
(51) Kamith, U.; Shriver, J. W. *J. Biol. Chem.* **1989**, *264*, 5586–5592.
(52) Jacobsen, J. P.; Bildsöe, H. K.; Schaumburg, K. *J. Magn. Reson.* **1976**, *23*, 153–164.
(53) Mittermaier, A.; Kay, L. E. *J. Am. Chem. Soc.* **1999**, *121*, 10608–10613.

(54) Lipari, G.; Szabo, A. *J. Am. Chem. Soc.* **1982**, *104*, 4559–4570.
(55) Woessner, D. E. *J. Chem. Phys.* **1962**, *37*, 647–654.
(56) Vijay-Kumar, S.; Bugg, C. E.; Cook, W. J. *J. Mol. Biol.* **1987**, *194*, 531–544.
(57) Xue, Y.; Pavlova, M. S.; Ryabov, Y. E.; Reif, B.; Skrynnikov, N. R. *J. Am. Chem. Soc.* **2007**, *129*, 6827–6838.
(58) Showalter, S. A.; Johnson, E.; Rance, M.; Brüschweiler, R. *J. Am. Chem. Soc.* **2007**, *129*, 14146–14147.
(59) Esadze, A.; Li, D. W.; Wang, T.; Brüschweiler, R.; Iwahara, J. *J. Am. Chem. Soc.* **2011**, *133*, 909–919.
(60) Clore, G. M.; Szabo, A.; Bax, A.; Kay, L. E.; Driscoll, P. C.; Gronenborn, A. M. *J. Am. Chem. Soc.* **1990**, *112*, 4989–4991.
(61) Choy, W. Y.; Kay, L. E. *J. Biomol. NMR* **2003**, *25*, 325–333.
(62) Xu, J.; Xue, Y.; Skrynnikov, N. R. *J. Biomol. NMR* **2009**, *45*, 57–72.
(63) Sheppard, D.; Li, D. W.; Brüschweiler, R.; Tugarinov, V. *J. Am. Chem. Soc.* **2009**, *131*, 15853–15865.
(64) Cho, C. H.; Urquidi, J.; Singh, S.; Robinson, G. W. *J. Phys. Chem. B* **1999**, *103*, 1991–1994.
(65) Tjandra, N.; Feller, S. E.; Pastor, R. W.; Bax, A. *J. Am. Chem. Soc.* **1995**, *117*, 12562–12566.
(66) Long, D.; Li, D. W.; Walter, K. F.; Griesinger, C.; Brüschweiler, R. *Biophys. J.* **2011**, *101*, 910–915.
(67) van der Spoel, D.; Lindahl, E.; Hess, B.; Groenhof, G.; Mark, A. E.; Berendsen, H. J. *J. Comput. Chem.* **2005**, *26*, 1701–1718.
(68) Jorgensen, W. L.; Chandrasekhar, J.; Madura, J. D.; Impey, R. W.; Klein, M. L. *J. Chem. Phys.* **1983**, *79*, 926–935.
(69) Lindorff-Larsen, K.; Piana, S.; Palmo, K.; Maragakis, P.; Klepeis, J. L.; Dror, R. O.; Shaw, D. E. *Proteins* **2010**, *78*, 1950–1958.
(70) Li, D.-W.; Brüschweiler, R. *Angew. Chem., Int. Ed. Engl.* **2010**, *49*, 6778–6780.
(71) Long, D.; Brüschweiler, R. *PLoS Comput. Biol.* **2011**, *7*, e1002035.
(72) Redfield, A. G. *IBM J. Res. Dev.* **1957**, *1*, 19–31.
(73) Ollerenshaw, J. E.; Tugarinov, V.; Skrynnikov, N. R.; Kay, L. E. *J. Biomol. NMR* **2005**, *33*, 25–41.
(74) Werbelow, L. G.; Allouche, A.; Pouzard, G. *J. Phys. Chem.* **1984**, *88*, 4692–4696.
(75) Werbelow, L. G.; Morris, G. A.; Kumar, P.; Kowalewski, J. *J. Magn. Reson.* **1999**, *140*, 1–8.
(76) Lee, A. L.; Sharp, K. A.; Kranz, J. K.; Song, X. J.; Wand, A. J. *Biochemistry* **2002**, *41*, 13814–13825.
(77) Chou, J. J.; Case, D. A.; Bax, A. *J. Am. Chem. Soc.* **2003**, *125*, 8959–8966.
(78) Bevington, P. R.; Robinson, D. K. *Data Reduction and Error Analysis for the Physical Sciences*; WCB/McGraw-Hill: New York, 1992.
(79) Del Rio, A.; Anand, A.; Ghose, A. *J. Magn. Reson.* **2006**, *180*, 1–17.
(80) Beal, R.; Deveraux, Q.; Xia, G.; Rechsteiner, M.; Pickart, C. *Proc. Natl. Acad. Sci. U.S.A.* **1996**, *93*, 861–866.
(81) Haas, A. L.; Siepmann, T. J. *FASEB J.* **1997**, *11*, 1257–1268.
(82) Massi, F.; Grey, M. J.; Palmer, A. G. *Protein Sci.* **2005**, *14*, 735–742.
(83) Nicholson, L. K.; Kay, L. E.; Baldisseri, D. M.; Arango, J.; Young, P. E.; Bax, A.; Torchia, D. A. *Biochemistry* **1992**, *31*, 5253–5263.
(84) Nicholson, L. K.; Kay, L. E.; Torchia, D. A. In *NMR spectroscopy and its applications to biomedical research*; Sarkar, S. K., Ed.; Elsevier: New York, 1996; pp 241−279.
(85) Song, X. J.; Flynn, P. F.; Sharp, K. A.; Wand, A. J. *Biophys. J.* **2007**, *92*, L43–45.
(86) Vugmeyster, L.; Trott, O.; McKnight, C. J.; Raleigh, D. P.; Palmer, A. G. *J. Mol. Biol.* **2002**, *320*, 841–854.
(87) Farès, C.; Lakomek, N. A.; Walter, K. F.; Frank, B. T.; Meiler, J.; Becker, S.; Griesinger, C. *J. Biomol. NMR* **2009**, *45*, 23–44.
(88) Howard, B. R.; Endrizzi, J. A.; Remington, S. J. *Biochemistry* **2000**, *39*, 3156–3168.
(89) Tugarinov, V.; Muhandiram, R.; Ayed, A.; Kay, L. E. *J. Am. Chem. Soc.* **2002**, *124*, 10025–10035.